Article

Cell

An Acquired Vulnerability of Drug-Resistant Melanoma with Therapeutic Potential

Graphical Abstract

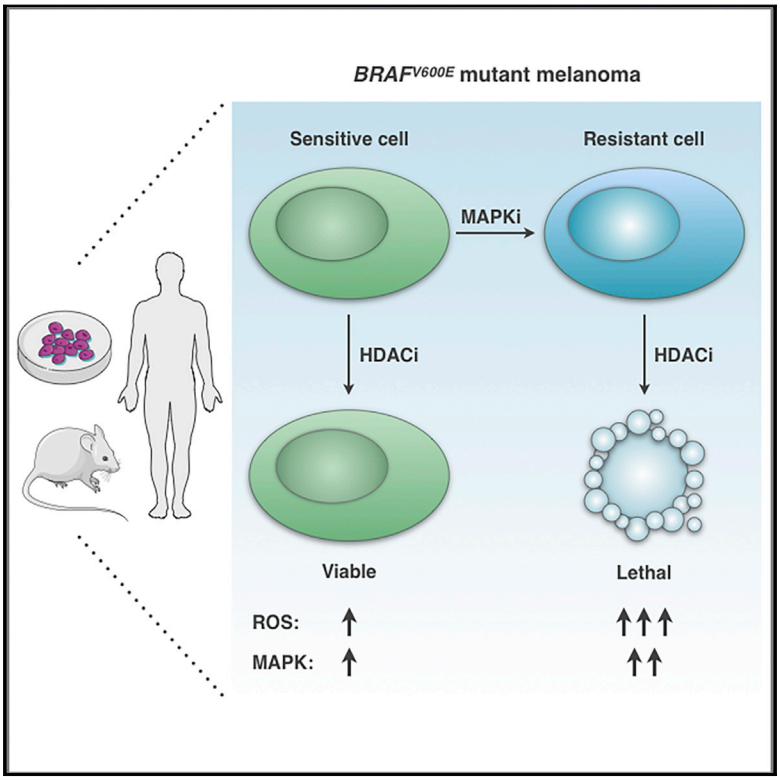

Authors

Liqin Wang, Rodrigo Leite de Oliveira, Sanne Huijberts, ..., Jos H. Beijnen, Jan H.M. Schellens, Rene Bernards

Correspondence

r.bernards@nki.nl

In Brief

Collateral sensitivity in BRAF inhibitor-resistant melanoma may confer selective vulnerability to histone deacetylase inhibitors.

Highlights

- BRAF inhibitor-resistant melanomas have elevated ROS levels
- Histone deacetylase inhibitors increase ROS levels through suppression of SLC7A11
- BRAF inhibitor resistance causes vulnerability to histone deacetylase inhibitors
- In patients, histone deacetylase inhibitors selectively kill drug-resistant cells

Wang et al., 2018, Cell *173*, 1413–1425
May 31, 2018
https://doi.org/10.1016/j.cell.2018.04.012

CellPress

Article

Cell

An Acquired Vulnerability of Drug-Resistant Melanoma with Therapeutic Potential

Liqin Wang,[1,5] Rodrigo Leite de Oliveira,[1,5] Sanne Huijberts,[2] Evert Bosdriesz,[1] Nora Pencheva,[1] Diede Brunen,[1] Astrid Bosma,[1] Ji-Ying Song,[3] John Zevenhoven,[3] G. Tjitske Los-de Vries,[1] Hugo Horlings,[1] Bastiaan Nuijen,[4] Jos H. Beijnen,[4] Jan H.M. Schellens,[2] and Rene Bernards[1,6,*]

[1]Division of Molecular Carcinogenesis, Oncode Institute, the Netherlands Cancer Institute, 1066 CX Amsterdam, the Netherlands
[2]Division of Clinical Pharmacology, Oncode Institute, the Netherlands Cancer Institute, 1066 CX Amsterdam, the Netherlands
[3]Division of Molecular Genetics, the Netherlands Cancer Institute, 1066 CX Amsterdam, the Netherlands
[4]Department of Pharmacy and Pharmacology, the Netherlands Cancer Institute, 1066 CX Amsterdam, the Netherlands
[5]These authors contributed equally
[6]Lead Contact
*Correspondence: r.bernards@nki.nl
https://doi.org/10.1016/j.cell.2018.04.012

SUMMARY

BRAF(*V600E*) mutant melanomas treated with inhibitors of the BRAF and MEK kinases almost invariably develop resistance that is frequently caused by reactivation of the mitogen activated protein kinase (MAPK) pathway. To identify novel treatment options for such patients, we searched for acquired vulnerabilities of MAPK inhibitor-resistant melanomas. We find that resistance to BRAF+MEK inhibitors is associated with increased levels of reactive oxygen species (ROS). Subsequent treatment with the histone deacetylase inhibitor vorinostat suppresses *SLC7A11*, leading to a lethal increase in the already-elevated levels of ROS in drug-resistant cells. This causes selective apoptotic death of only the drug-resistant tumor cells. Consistently, treatment of BRAF inhibitor-resistant melanoma with vorinostat in mice results in dramatic tumor regression. In a study in patients with advanced BRAF+MEK inhibitor-resistant melanoma, we find that vorinostat can selectively ablate drug-resistant tumor cells, providing clinical proof of concept for the novel therapy identified here.

INTRODUCTION

Approximately half of melanoma skin cancers carry activating mutations in the *BRAF* oncogene, leading to activation of the mitogen-activated protein kinase (MAPK) pathway. Inhibition of the BRAF oncoprotein by targeted drugs provides substantial benefit to patients, albeit most patients ultimately relapse with resistant disease (Sosman et al., 2012). Dual inhibition of both BRAF and the downstream MEK kinases leads to more sustained clinical benefit, but resistance is still mostly inevitable (Robert et al., 2015). Resistance to MAPK pathway inhibitors in melanoma is frequently caused by reactivation of signaling through this pathway in the presence of drug (Van Allen et al., 2014; Wagle et al., 2014). Multiple mechanisms of MAPK reactivation have been described, including upregulation of receptor tyrosine kinases (RTKs), mutations in *KRAS* and *NRAS*, splice site mutations in *BRAF*, amplification of *BRAF*, and mutation of MEK kinases (reviewed by Manzano et al. [2016]). Drug withdrawal in such drug-resistant patients often does not lead to an immediate disease flare up, but rather to a transient pause in tumor growth, known as the "drug holiday effect" (Seghers et al., 2012). This effect can be explained, at least in part, by hyper-activation of the MAPK pathway signaling following drug withdrawal, leading to a cellular state that has hallmarks of oncogene-induced senescence (Sun et al., 2014). Downregulation of this hyper-active MAPK signaling marks the end of the drug holiday, resulting in reinitiation of tumor growth and regained drug sensitivity upon rechallenge with BRAF inhibitor (Seghers et al., 2012).

The transient proliferation arrest of BRAF inhibitor-resistant melanomas following drug withdrawal points to an acquired vulnerability of drug-resistant cells that was not present in the parental drug-sensitive cells (Sun et al., 2014). That drug resistance of cancer cells comes at a fitness cost that in turn can cause sensitivity to other drugs was identified over 50 years ago and is referred to as "collateral sensitivity" (Hutchison, 1963). Previous studies have pointed to alterations in mitochondrial oxidative metabolism when signaling through the MAPK pathway is modulated (Baenke et al., 2016; Corazao-Rozas et al., 2013; Haq et al., 2013; Hernandez-Davies et al., 2015; Vazquez et al., 2013). Here, we report a collateral sensitivity of BRAF inhibitor-resistant melanoma that takes advantage of increased levels of reactive oxygen species (ROS) in drug-resistant cells.

RESULTS

A Vulnerability of MAPKi-Resistant Melanoma

To explore new therapeutic strategies for melanomas having acquired resistance to inhibitors of the MAPK pathway, we

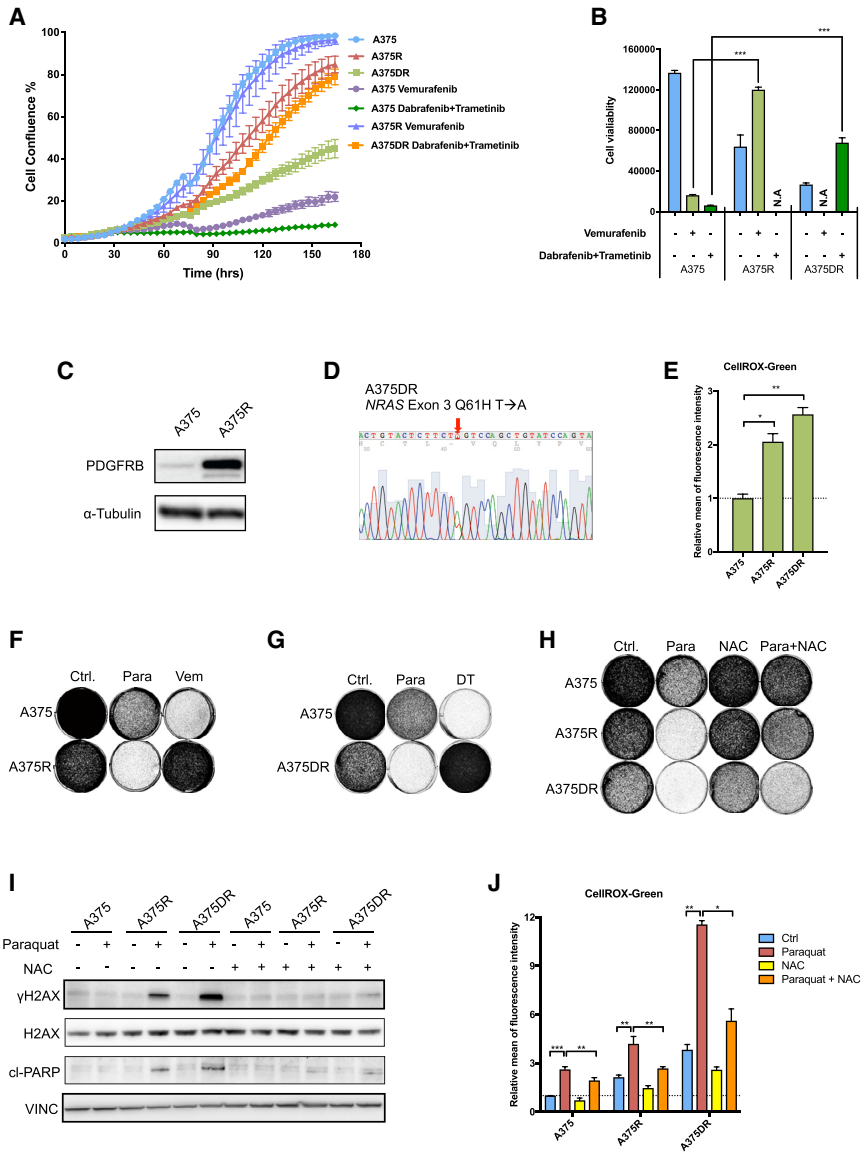

Figure 1. ROS Levels and ROS Sensitivity of Melanoma Cells

(A) Incucyte proliferation assays of parental (A375), BRAFi-resistant (A375R), and BRAFi/MEKi double-resistant (A375DR) melanoma cells in the presence or absence of 2 μM vemurafenib or combination of 0.5 μM dabrafenib and 10 nM trametinib.

(B) Quantification of cell viability assay of parental and drug-resistant cells cultured in the presence or absence of MAPK inhibitors shown in (A) at the end of the assay. Cell viability was quantified with CellTiter-Blue.

(C) Western blot analysis of *PDGFRB* expression in A375 cells and A375R cells.

(D) Sanger sequencing analysis of NRAS gene in A375DR cells showing gain of $NRAS^{Q61H}$ mutation.

(E) ROS levels of A375R, A375DR, and parental A375 cells measured after 72 hr of culturing without drugs. ROS levels were measured using CellROX-Green flow cytometry assay. Relative ROS levels are plotted.

(F and G) Long-term colony formation assays of A375R (F) and A375DR (G) compared to parental A375 cells treated with paraquat and/or MAPK inhibitors (Vem, vemurafenib; DT, dabrafenib+trametinib). Cells were seeded 50,000 cells per well in 6-well plates and treated with 20 μM paraquat, 2 μM vemurafenib, or a combination of 10 nM trametinib and 0.5 μM dabrafenib for 10 days. Afterward, the cells were fixed, stained, and photographed.

(H) Long-term colony formation assays of parental and MAPKi-resistant A375 cells treated with paraquat and/or NAC. Cells were seeded 50,000 cells per well in 6-well plates and treated with 20 μM paraquat and/or 2.5 mM N-acetyl-L-cysteine (NAC) for 10 days. Afterward, the cells were fixed, stained, and photographed.

(I) Protein lysates were harvested from the MAPKi-resistant (R and DR cells), and parental A375 cells were treated with 25 μM paraquat and/or 2.5 mM NAC for 72 hr. Western blot analysis of γH2AX as a DNA damage marker and cleaved-PARP (cl-PARP) as an apoptosis marker; vinculin (VINC) served as the loading control.

(J) Parental and MAPKi-resistant A375 cells were treated with 20 μM paraquat and/or 2.5 mM NAC for 72 hr. ROS levels were measured using CellROX-Green flow cytometry assay.

Error bars represent the mean ± SD from the biological triplicates (*$p \leq 0.05$, **$p \leq 0.01$, ***$p \leq 0.001$, Student's t test).

See also Figure S1.

generated drug-resistant derivatives of *BRAF* mutant A375 human melanoma cells by long-term culture in the presence of the BRAF inhibitor vemurafenib (A375R, resistant cells) or a combination of the BRAF inhibitor dabrafenib and the MEK inhibitor trametinib (A375DR, double-resistant cells). In a short-term proliferation assay, A375R and A375DR cells proliferated in the presence of vemurafenib and the combination of dabrafenib plus trametinib, respectively, whereas parental A375 cells were sensitive to MAPK inhibition (Figure 1A). In the absence of MAPK inhibitors (MAPKi), A375R and A375DR cells displayed slight proliferation impairment, modeling the drug holiday effect seen in the clinic (Seghers et al., 2012). Quantification of cell viability at the end of the proliferation assay confirmed the sustained viability of the MAPKi-resistant A375R and A375DR derivatives in the presence of the drugs (Figure 1B). Further characterization of these derivatives revealed that A375R cells have gained platelet-derived growth factor receptor B (*PDGFRB*) expression (Figure 1C), while A375DR cells acquired a secondary $NRAS^{Q61H}$ mutation (Figure 1D). Similar results were obtained in Mel888 cells, another $BRAF^{V600E}$ mutated human melanoma model. After a similar long-term culture protocol in MAPKi, we isolated a variant resistant to vemurafenib (Mel888R) (Figures S1A and S1C) and a line resistant to the combination of dabrafenib plus trametinib (Mel888DR) (Figures S1B

and S1C). Mel888R cells express a splice variant of *BRAF* (Figure S1D), whereas Mel888DR harbor a secondary $KRAS^{G12C}$ mutation (Figure S1E). These four resistance mutations commonly found in melanoma patients that develop resistance to drugs that target BRAF and/or MEK kinases converge on the hyper-activation of the MAPK pathway. These data also underscore that, although generated *in vitro*, our drug-resistant melanoma cell line derivatives faithfully recapitulate clinical drug resistance.

One of the features of increased RAS signaling is the abundant production of ROS, which serve as signaling molecules in multiple cellular pathways (Lee et al., 1999; Reczek and Chandel, 2017; Ruefli et al., 2001). To test whether this is also the case in melanoma, we measured ROS levels using fluorescent flow cytometry. Indeed, basal levels of ROS were 2-fold higher in single drug-resistant cells (A375R and Mel888R) and increased even further in double drug-resistant cells (A375DR and Mel888DR) (Figures 1E and S1F). We hypothesized that this increase in ROS levels may represent an acquired vulnerability in the sense that a further increase in ROS levels could become detrimental to the drug-resistant cells. To test this, we exposed parental and drug-resistant melanoma cells to the ROS inducer paraquat. Indeed, paraquat treatment inhibited the proliferation of single-resistant A375R cells and double-resistant A375DR cells in a colony formation assay, while it induced only slight proliferation impairment in the parental cells (Figures 1F, 1G, S1G, and S1H). The sensitivity to paraquat in resistant melanoma cells was proportional to the higher basal ROS levels (Figures 1E and S1F) and correlated with an increase of DNA damage and apoptosis, as evidenced by the presence of γ-H2AX and cleaved PARP, respectively (Figures 1I and S1J). The notion that increased sensitivity of MAPKi-resistant cells to paraquat is mediated by increased ROS levels is supported by the observation that treatment with the ROS scavenger N-acetyl-cysteine (NAC) reduced ROS levels negated the sensitivity of BRAFi-resistant cells to paraquat (Figures 1H and S1I) and reduced DNA damage and apoptosis (Figures 1I, 1J, S1J, and S1K). These findings indicate that regardless of the type of mutation responsible for acquired MAPKi-resistance in melanomas, ROS induction is a common vulnerability that can be targeted with ROS inducers.

MAPKi-Resistant Melanoma Cells Are Sensitive to Vorinostat

To take this concept closer to a potential clinical use, we searched for approved drugs that also induce ROS. We selected histone deacetylase inhibitor (HDACi) vorinostat, because vorinostat has a safe pharmacological profile in the clinic and HDACi are known to induce ROS (Petruccelli et al., 2011; Ruefli et al., 2001; Ungerstedt et al., 2005; Wolf et al., 2014). To test whether vorinostat also induces ROS in melanoma, we treated our two cell models with vorinostat for 72 hr and measured intracellular ROS. Indeed, vorinostat induced ROS levels in parental and resistant cells, which could be prevented by co-treatment with NAC (Figures 2A and S2A). In long-term proliferation assays, vorinostat treatment inhibited the growth of drug-resistant cells, but the combination of vorinostat and NAC rescued this effect in both melanoma models (Figures 2B and S2B). Again, the vorinostat effect was far more pronounced in MAPKi-resistant melanoma cells, as it only caused mild proliferation impairment in parental cells, also in a short-term Incucyte assay (Figures 2C and S2C). The differential effect of vorinostat is most likely explained by the much higher ROS levels induced in MAPKi-resistant melanoma cells as compared to the ROS levels induced by vorinostat in parental cells (Figures 2A and S2A). Similar to paraquat treatment, vorinostat induced DNA damage and apoptosis in BRAFi-resistant, but not in parental A375 cells, which was rescued by NAC treatment (Figure 2D). In Mel888 cells, vorinostat treatment also induced apoptosis in MAPKi-resistant cells (Mel888R and Mel888DR) but not in the parental line (Figure S2D). The same results were essentially obtained with a second ROS scavenger glutathione ethyl ester (GEE) as GEE also reduced ROS levels induced by vorinostat and rescued the proliferation defect induced by vorinostat in MAPK inhibitor-resistant cells (Figures 2E, 2F, S2E, and S2F). These observations suggest that a certain ROS level is required to inflict sufficient DNA damage and to activate cell death pathways, which is only achieved by vorinostat in drug-resistant, but not in parental, melanoma cells.

We also tested the vorinostat sensitivity in *NRAS* mutant melanoma cells, since this gene is the second most commonly mutated in melanoma patients. We generated *NRAS* mutant SK-MEL-147 melanoma cells resistant to MEK inhibitor by long-term culture in trametinib-containing medium. Vorinostat treatment of parental SK-MEL-147 cells and resistant derivatives (SK-MEL-147R) induced an increase in intracellular ROS levels that could be abrogated with co-treatment with NAC (Figure S2G). Accordingly, in a colony formation assay SK-MEL-147R cells showed increased sensitivity to vorinostat as compared to the parental line. This sensitivity was reversed by the concomitant treatment with NAC (Figure S2H).

MAPK Inhibition Is Antagonized by HDACi

It has been shown in short-term assays that combined HDAC and MAPK inhibition can prevent some forms of MAPK inhibitor resistance in melanoma (Johannessen et al., 2013). It also has been shown, however, that increased ROS levels lead to activation of the MAPK pathway (Son et al., 2011). This would suggest that vorinostat, by virtue of its increase in ROS levels, could activate MAPK signaling and thereby counteract the effects of MAPK inhibitors. Indeed, also in melanoma, vorinostat activated MAPK signaling in A375, A375R, and A375DR cells, as evidenced by an increase in phosphorylated MEK (pMEK) and p-P90RSK (Figures 3A and 3B). While MAPK inhibitors were able to reduce levels of pMEK and p-P90RSK in all three cells, combined treatment with MAPKi and vorinostat resulted in significant residual MAPK signaling (Figures 3A and 3B). Consistent with this, treatment of A375 or Mel888 cells with a combination of HDACi and MAPKi resulted in continued proliferation (Figures 3C and S3C). Conversely, whereas A375DR and A375R are hypersensitive to three different HDAC inhibitors, the combination of MAPKi and HDACi resulted in a poor response (Figures 3C and 3D). This finding is most readily explained by the reduced MAPK signaling caused by the MAPKi, resulting in lower ROS levels and hence a lesser effect of ROS increase by HDACi. Indeed, treatment of A375 and A375 DR cells with MAPK

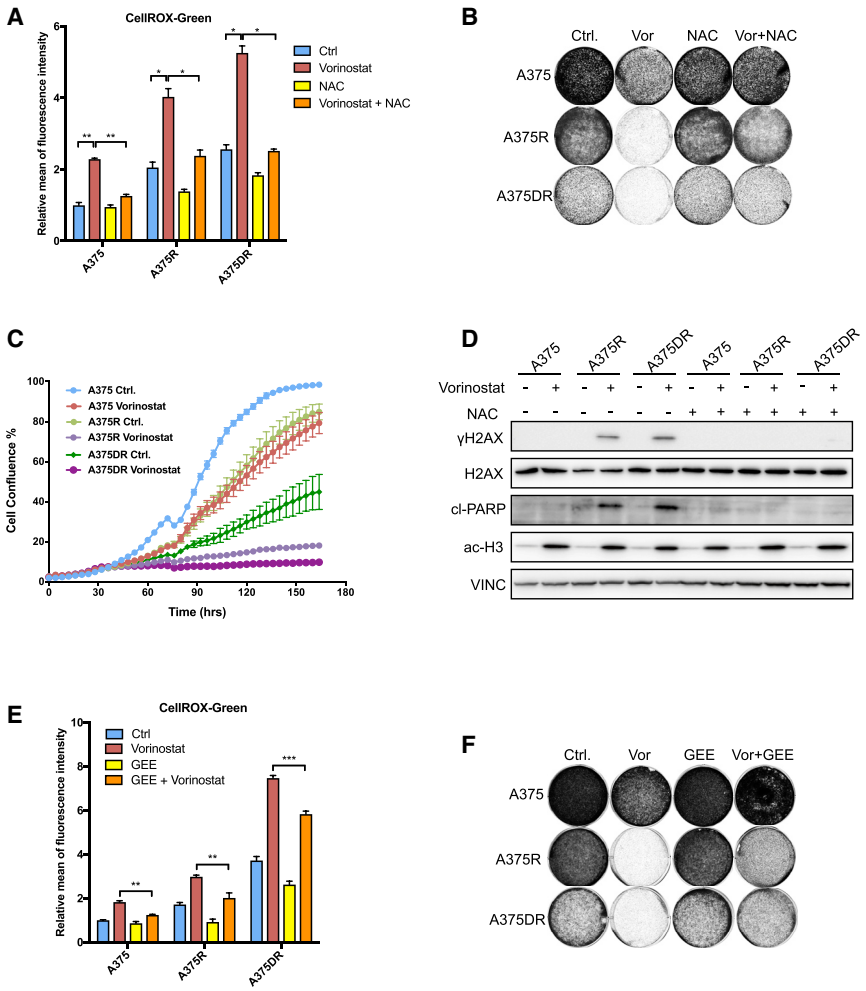

Figure 2. HDACi Is Detrimental to MAPKi-Resistant Melanoma Cells

(A) Parental and MAPKi-resistant A375 cells were treated with 2 μM vorinostat and/or 2.5 mM NAC for 72 hr. ROS levels were measured using CellROX-Green flow cytometry assay. Relative ROS levels are indicated.

(B) Long-term colony formation assays of parental and MAPKi-resistant A375 cells treated with vorinostat and/or NAC. Cells were seeded 50,000 cells per well in 6-well plates and treated with 1 μM vorinostat and/or 2.5 mM NAC for 8 days. Afterward, the cells were fixed, stained, and photographed.

(C) Incucyte proliferation assay of parental and MAPKi-resistant A375 cells were seeded 400 cells per well in a 384-well plate and cultured in the presence or absence of 1 μM vorinostat.

(D) Protein lysates were harvested from the MAPKi-resistant and parental A375 cells treated with 1 μM vorinostat and/or 2.5 mM NAC for 72 hr, and western blot analysis was performed for gamma-H2AX (γH2AX) as a DNA damage marker and cleaved-PARP (cl-PARP) as an apoptosis marker. Ac-H3 was used as an indicator for levels of acetylated histone H3. Vinculin (VINC) served as the loading control.

(E) Parental and MAPKi-resistant A375 cells were treated with 2 μM vorinostat and/or 2.5 mM reduced glutathione ethyl ester (GEE) for 72 hr. ROS levels were measured using CellROX-Green flow cytometry assay. Relative ROS levels are indicated.

(F) Long-term colony formation assays of parental and MAPKi-resistant A375 cells treated with vorinostat and/or GEE. Cells were seeded 50,000 cells per well in 6-well plates and treated with 1 μM vorinostat and/or 2.5 mM GEE for 8 days. Afterward, the cells were fixed, stained, and photographed.

Error bars represent the mean ± SD from the biological triplicates (*$p \leq 0.05$, **$p \leq 0.01$, ***$p \leq 0.001$, Student's t test).

See also Figure S2.

inhibitors reduced ROS levels and suppressed the increase in ROS caused by vorinostat (Figures 3E and 3F). The same results were essentially obtained in short-term proliferation assays (Figures 3G–3L), in additional *BRAF*^{V600E} mutant melanomas (Figures S3C–S3G), and in the *NRAS* mutant melanoma models (Figure S3H).

To further study the antagonism of ROS and MAPK inhibition, we performed long-term colony formation on A375 cells treated with the BRAFi vemurafenib and/or the ROS inducer paraquat. Figures 3M and S3I show that the ROS inducers paraquat and DMNQ inhibit the proliferation of the cells in a dose-dependent manner, but this was counteracted by vemurafenib. Moreover, paraquat and *tert*-butyl-hydroperoxide (tBHP, another ROS inducer) both caused an increase in RAS-GTP loading in A375 cells and prevented vemurafenib from effectively inhibiting MEK activity (Figures 3N and 3O). These results indicate that indeed ROS can positively regulate MAPK signaling, as previously shown by others (Son et al., 2011). Consistently, vorinostat can increase RAS-GTP loading in A375, but this induction can be abrogated by co-treatment with the ROS scavenger NAC (Figure 3P). Taken together, these data indicate antagonistic effects of HDACi and MAPKi and emphasize the need to administer MAPK and HDAC inhibitors sequentially in a therapeutic setting rather than simultaneously, a notion that is tested further below.

HDACi Confers a Disadvantage to MAPKi-Resistant Melanoma

We have shown previously that acquisition of resistance to vemurafenib leads to a transient proliferation arrest upon drug withdrawal, phenocopying the transient arrest in tumor growth upon drug withdrawal seen in the clinic, known as the drug holiday effect (Seghers et al., 2012; Sun et al., 2014). Biochemically, vemurafenib withdrawal in drug-resistant cells resulted in hyperactivation of the MAPK pathway and indeed such cells have hallmarks of "oncogene-induced senescence" (Sun et al., 2014). Our present data indicate that treatment of MAPKi-resistant melanoma with HDACi results in active cell death, suggesting that this treatment is more effective in MAPKi-resistant melanoma than in drug-sensitive cells. We tested this prediction in a competition assay using a mixed population of parental and

two MAPKi-resistant derivatives (R and DR) of A375 cells and Mel888 cells. Drug-sensitive and drug-resistant cells were labeled with green or red fluorescent proteins through transduction with lentiviral vectors encoding GFP and RFP. The two cell populations were mixed in a 1:9 or 1:8 ratio of drug-resistant cells over drug sensitive cells and cultured with no drug (drug holiday effect), MAPKi, or HDACi, as schematically outlined in Figure 4A. Relative abundance of the two populations was followed over 17 days using quantification by flow cytometry. Figure 4B shows that MAPK inhibition efficiently depleted GFP+ parental cells and enriched RFP+ MAPKi-resistant cells. In contrast, RFP+ MAPKi-resistant cells were depleted by vorinostat treatment, while GFP+ parental cells were enriched. The drug holiday arm followed the same trend as the vorinostat arm; however, the changes were moderate and initiated at a later time point (Figures 4B, 4C, S4A, and S4B). These results support the notion that a switch from MAPKi to HDACi can specifically deplete the drug-resistant cells in a heterogeneous melanoma population that harbors both drug sensitive and drug-resistant cells. Moreover, the competition experiment indicates that a switch to HDACi upon development of resistance to MAPKi is more effective in eliminating drug-resistant cells than a drug holiday.

HDACi Induces ROS through Suppression of SLC7A11

To systematically interrogate the molecular pathways governing ROS induction upon HDACi treatment, we performed transcriptome profiling by next-generation RNA sequencing (RNA-seq) of A375 parental and MAPKi-resistant derivatives (A375R and A375DR) treated with and without vorinostat. This analysis identified a set of 12 genes commonly downregulated in the three cell lines upon HDACi treatment (Table S1). We focused our attention on *SLC7A11*, as it encodes the cystine-glutamate antiporter xCT. This transporter is responsible for the cellular intake of cystine, the precursor of the major antioxidant glutathione (GSH) (Bannai and Tateishi, 1986; Gout et al., 1997). Suppression of this antiporter can therefore lead to reduction of cellular GSH levels and, consequently, increased cellular ROS. To investigate whether HDACi can induce ROS through *SLC7A11* suppression in *BRAF* or *NRAS* mutant melanomas, we first quantified changes in *SLC7A11* expression upon treatment of parental and resistant melanoma cells with HDACi using qRT-PCR. Vorinostat indeed transcriptionally suppressed *SLC7A11* in three melanoma models (Figures 5A, S5A, and S5I) and reduced GSH levels in two melanoma models (Figures 5B and S5B). In addition, genetic silencing of *SLC7A11* using multiple short hairpin RNAs (shRNAs) increased melanoma ROS levels (Figures 5C and 5D). These shRNAs also suppressed proliferation in our melanoma models, in particular the double-resistant cells (Figures 5E and S5D). Next, we used the most efficient shRNA (shSLC7A11-4) to study the effect of *SLC7A11* reduction on ROS induction. We observed that *SLC7A11* suppression correlated with increased ROS levels both in the parental cells and also in the MAPKi-resistant derivatives (Figures 5F, 5G, S5C, and S5E). This suggests that the HDACi-mediated ROS induction is (at least in part) due to the reduction of *SLC7A11* expression in melanomas, leading to reduced GSH levels. The ROS scavenger trolox acts on the lipid peroxidation process only and did not affect ROS levels in A375R and A375DR cells and did not rescue the toxicity of vorinostat in these cells (Valko et al., 2007) (Figures S5M and S5N). Glutathione in contrast acts more broadly on oxygen radicals and therefore is more efficient in rescuing increased ROS in melanoma (see also Figures 2E and S2E). To further support the notion that *SLC7A11* is responsible for ROS modulation by HDACi, we overexpressed *SLC7A11* using a lentiviral vector, leading to a 25- to 30-fold increase in *SLC7A11* mRNA levels (Figure 5I). Our data predict that *SLC7A11* overexpression should rescue the HDACi-mediated ROS induction and consequently also the anti-proliferation effect of vorinostat. The short-term IncuCyte proliferation assay (Figures 5J and 5K) and long-term colony formation assay (Figures 5L and S5G) indicate that the HDACi-mediated anti-proliferation effect is reduced by *SLC7A11* overexpression. Quantification of the short-term proliferation assays are shown in Figure S5O. Moreover, HDACi-mediated ROS induction was abrogated by *SLC7A11* overexpression (Figures 5M and S5H). This same mechanism was confirmed in additional *NRAS* mutant melanoma (SK-MEL-147) models (Figures S5I–S5L).

In Vivo Study of Sequential Drug Treatment

Next, we tested the effectiveness of sequential treatment of melanoma with BRAFi, followed by a switch to HDACi upon progression on BRAFi *in vivo*. We injected immunodeficient nude mice with A375 cells and after tumors reached 500 mm^3, animals were fed a control chow, chow supplemented with PLX4720 (an analog of vemurafenib) or with vorinostat through daily intraperitoneal injection. Figure 6A shows that in the absence of drug or in the presence of vorinostat, A375 cells formed progressively growing tumors. In the presence of PLX4720 tumors regressed initially, but drug-resistant tumors started to emerge approximately 40-50 days after the start of PLX4720 treatment. To address which mechanisms of PLX4720 resistance operated *in vivo*, we re-established four drug-resistant A375 tumors in cell culture (*ex vivo* A1–A4, exv. A1–A4). Figure 6G shows that each of these four tumor-derived cell lines was highly resistant to vemurafenib, but responded to vorinostat, belinostat, and panobinostat. All four cell lines maintained elevated levels of p-MEK in the presence of vemurafenib (Figure 6C), which is explained by an amplification of *BRAF* in the case of exv. A4 cells and a gain of an $NRAS^{Q61K}$ mutation in the case of exv. A3 cells (Figures 6D and 6E). The other two drug-resistant tumor lines exhibited increased expression of bona fide transforming growth factor β (TGF-β) target genes, suggestive of the possibility of activated TGF-β signaling in these *ex vivo* clones (Figure 6F), which has also been linked to resistance to vemurafenib (Huang et al., 2012). These data indicate that a range of different mechanisms can operate *in vivo* to confer resistance to BRAF inhibition and that, like in actual patients, in most cases drug resistance results from reactivation of MAPK signaling. Most importantly, these data also indicate that melanoma cells with reactivated MAPK signaling are very responsive to HDACi, regardless of how MAPK signaling was reactivated.

To test directly in an animal model whether BRAFi-resistant melanomas are responsive to HDACi, we allowed the

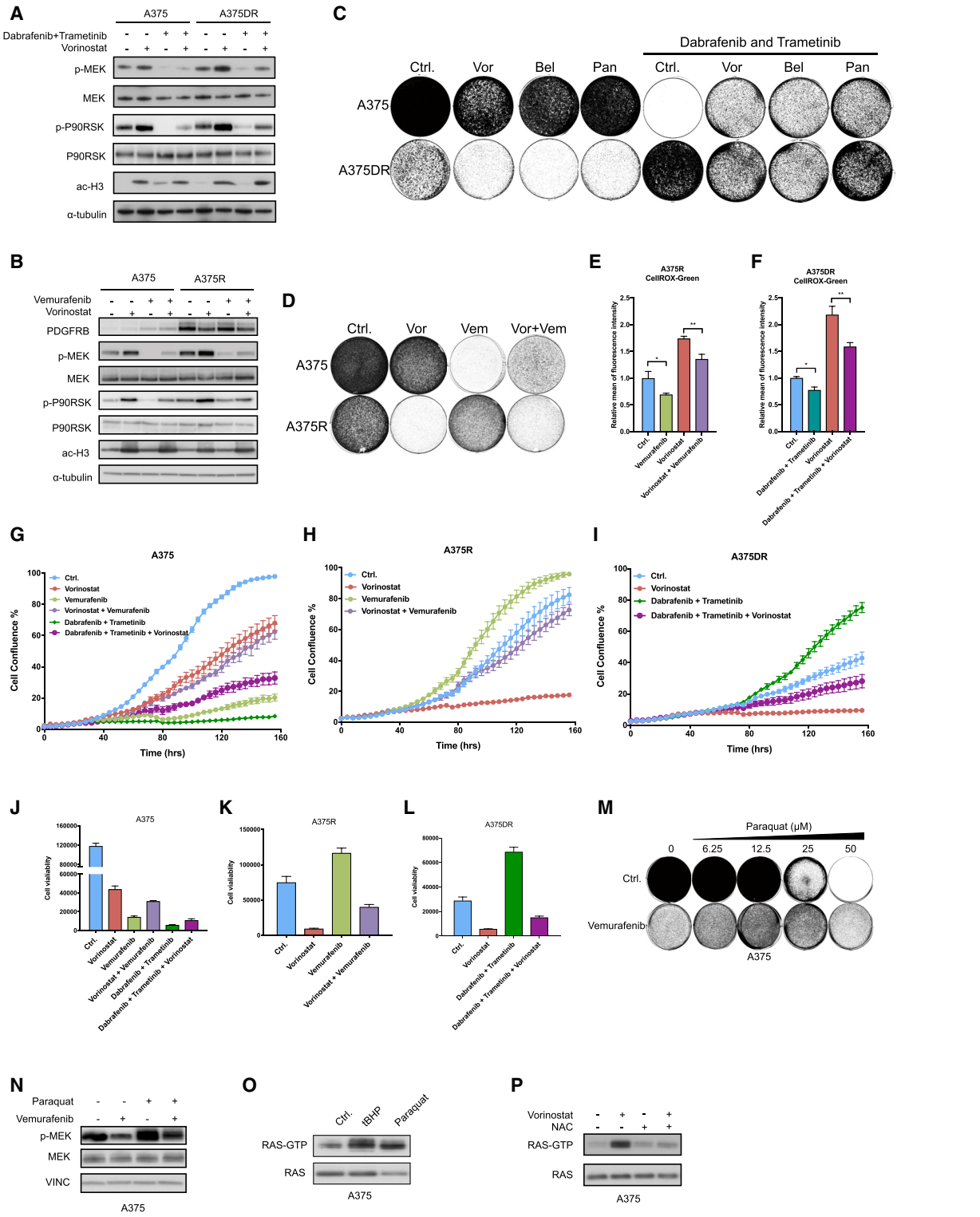

Figure 3. MAPK Inhibition Is Antagonistic with HDAC Inhibition

(A) BRAFi/MEKi-resistant A375DR and the parental A375 cells were treated with 2 μM vorinostat and/or the combination of 0.125 μM dabrafenib and 5 nM trametinib. Protein lysates were harvested after 72 hr. Western blot analysis was carried out for p-MEK and p-P90RSK as indicators of activation of MAPK pathway, ac-H3 as indicator for levels of acetylated histone H3 and α-tubulin as a loading control.

(legend continued on next page)

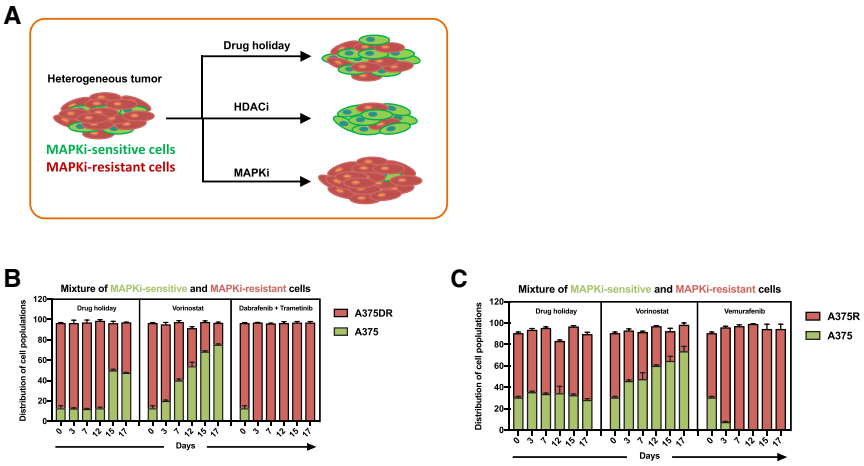

Figure 4. HDACi Is Detrimental to MAPKi-Resistant Melanoma

(A) Schematic of the *in vitro* competition assay to study the effect of HDAC inhibition in a heterogeneous tumor containing both MAPKi-resistant and MAPKi-sensitive cells. MAPKi-resistant cells were labeled with red fluorescent protein (RFP) through stable infection with a lentiviral vector pLKO-H2B-RFP. MAPKi-sensitive cells were labeled with GFP by infection with lentiviral vector pLKO-H2B-GFP. After mixing the MAPKi-resistant and sensitive cell populations, the cells were followed after different treatments. MAPK inhibition served as a control. MAPKi treatment resulted in enrichment of RFP+ cells.

(B and C) MAPKi-resistant A375DR cells (RFP+) (B) or A375R cells (C) were mixed at a 9-to-1 ratio with MAPKi-sensitive parental A375 cells (GFP+), and then 2,000,000 cells were seeded cells into 10-cm dishes and followed after different treatments. At each time point, the distribution of the cell populations was determined using flow cytometry. The ratio of the two cell population is indicated at the starting of the experiment (day 0). The distribution changes in the two cell populations are plotted on the y axis against the time on the x axis.

Error bars represent SD of the biological triplicates.

See also Figure S4.

PLX4720-treated tumors in our mouse cohort to acquire drug resistance (after tumors reached a volume of approximately 400 mm^3 in the presence of drug), which took on average 110 days (Figure 6A). After this, mice were randomized into four treatment cohorts: no drug, vorinostat only, PLX4720 only or the combination of vorinostat and PLX4720. Figure 6B shows the response of the PLX4720-resistant tumors to these four treatment regimens. Continuous PLX4720 treatment resulted in the most rapid tumor growth, consistent with the notion that these cells are fully drug-resistant. PLX4720 withdrawal resulted in a pausing of tumor growth followed by slow growth, analogous to the drug holiday effect seen in drug-resistant patients. A slow-growth phenotype was also seen for tumors treated with a combination of vorinostat and PLX4720, consistent with the notion that these two drugs are antagonistic. Most strikingly, a decline in tumor volume was seen when PLX4720-resistant tumors were switched to vorinostat alone, in agreement with the cytotoxic effects of HDACi on BRAFi-resistant melanoma cell lines seen *in vitro*.

Clinical Validation of Sequential Drug Treatment

To investigate the MAPKi-HDACi sequential treatment efficacy in patients, we initiated a clinical study (NCT02836548) to evaluate the effects of vorinostat treatment in $BRAF^{V600E}$ mutated advanced melanoma patients that had progressed on dabrafenib+trametinib therapy. We synthesized vorinostat under GMP conditions in our own pharmacy (see the STAR Methods). Since the *in vitro* studies demonstrated that HDACi and MAPKi act antagonistically, we used a 1-week MAPKi drug washout in patients before vorinostat administration. After this, patients received vorinostat in a safe single daily oral dose of 360 mg, slightly lower than the 400 mg dose approved for use in

(B) A375R and the parental cells were treated with 2 μM vorinostat and/or 0.5 μM vemurafenib for 72 hr, and after which protein lysates were harvested. Western blot analysis was performed for p-MEK and p-P90RSK as activation of MAPK pathway. ac-H3 indicated levels of acetylated histone H3 and PDGFRB. α-tubulin served as the loading control.

(C) A375DR and parental cells were seeded 50,000 cells per well in 6-well plates and treated with 1 μM vorinostat (Vor), 0.5 μM belinostat (Bel), 5 nM panobinostat (Pan), and/or combination of 5 nM trametinib and 0.125 μM dabrafenib.

(D) A375R and parental cells were seeded 50,000 cells per well in 6-well plates and treated with 1 μM vorinostat and/or 1 μM vemurafenib. After 10 days culturing, the cells were fixed, stained, and photographed.

(E and F) Relative ROS level meaurements of A375R treated with 2 μM vorinostat and/or 2 μM vemurafenib (E), A375DR cells with 2 μM vorinostst, and/or the combination of 0.125 μM dabrafenib and 5 nM trametinib (F).

(G–I) Incucyte proliferation assay of A375 cells (G), A375R cells (H), and A375DR (I) cells seeded at 400 cells per well in a 384-well plate cultured in the presence or absence of 1 μM vorinostat, 1 μM vemurafenib, and/or combination of 62.5 nM dabrafenib and 5 nM trametinib.

(J–L) At the end of the Incucyte assay, the cell viability of A375 cells (J), A375R cells (K), and A375DR cells (L) cells were quantified. Cell viability was measured with CellTiter-Blue.

(M) Long-term colony formation assays of A375 cells treated with 0.25 μM vemurafenib and indicated concentrations of paraquat for 10 days.

(N) A375 cells were treated with 50 μM paraquat and/or 0.25 μM vemurafenib, and protein lysates were harvested after 48 hr. Western blot analysis was performed for p-MEK and total MEK. Vinculin (VINC) served as the loading control.

(O) RAS-GTP loading measurement by western blot in A375 cells treated for 30 min with 125 mM tert-Butyl hydroperoxide (tBHP) or 48 hr of 50 μM paraquat treatments.

(P) RAS-GTP loading measurement by western blot in A375 cells treated with 2 μM vorinostat and/or 5 mM NAC for 72 hr.

Error bars represent the mean ± SD from the biological triplicates (*$p \leq 0.05$, **$p \leq 0.01$, ***$p \leq 0.001$, Student's t test).

See also Figure S3.

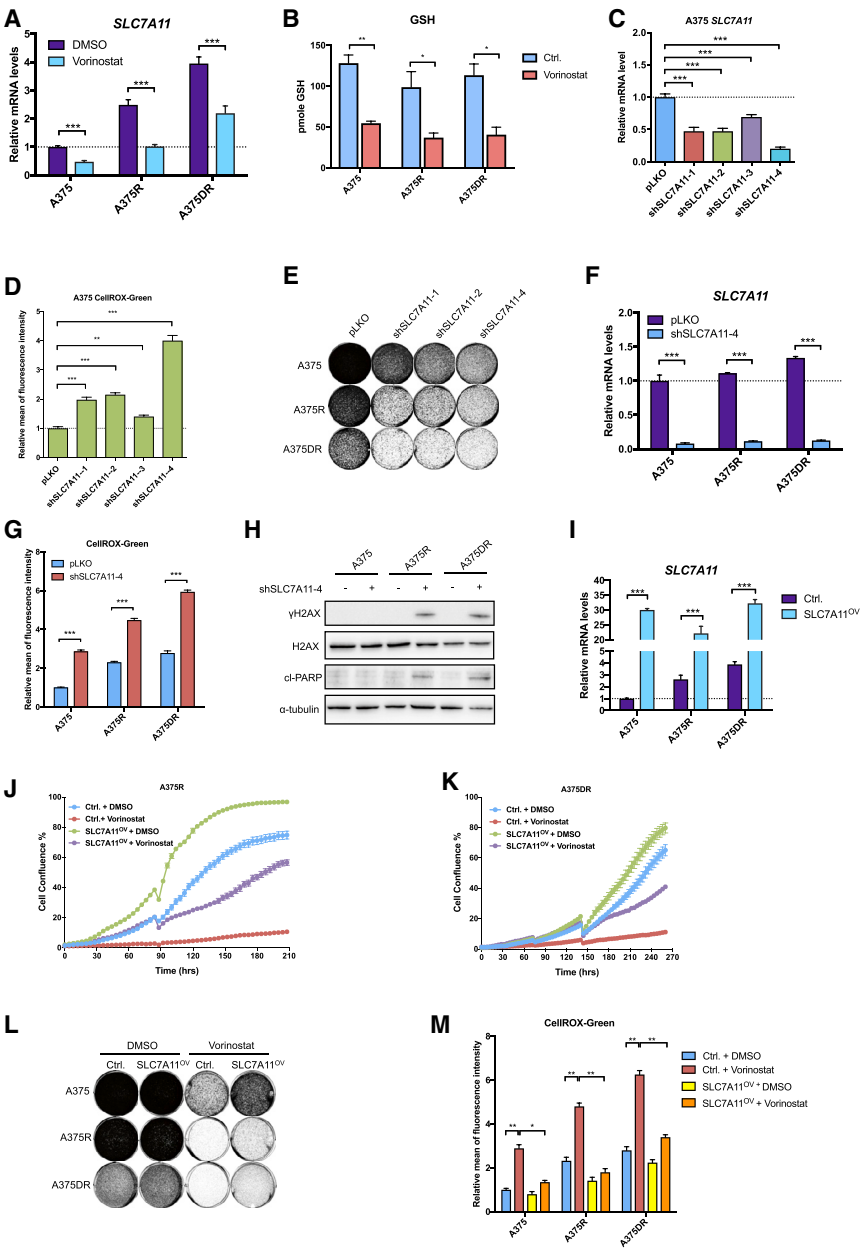

Figure 5. HDACi Suppresses *SLC7A11*, Resulting in ROS Induction

(A) mRNA expression analysis of *SLC7A11* by qRT-PCR in parental and MAPKi-resistant A375 cells treated with 2 μM vorinostat for 48 hr.

(B) Parental and MAPKi-resistant A375 cells were treated with 2 μM vorinostat for 72 hr. Total intracellular glutathione (GSH) levels were measured using a colorimetric-based glutathione detection assay.

(C) Four independent shRNAs targeting *SLC7A11* were individually introduced in A375 cells by lentiviral transduction. pLKO empty vector served as the control. The level of *SLC7A11* knockdown by each shRNAs was measured by qRT-PCR and is shown.

(D) Relative ROS induction upon *SLC7A11* knockdown as measured by flow cytometry.

(E) Long-term colony formation of parental and MAPKi-resistant A375 cells upon *SLC7A11* knockdown. The cells were seeded 50,000 cells per well in 6-well plate and cultured 10 days. Afterward, the cells were fixed, stained, and photographed.

(F) The levels of *SLC7A11* knockdown in parental and MAPKi-resistant A375 cells were measured by qRT-PCR.

(G) Relative ROS levels in parental and MAPKi-resistant A375 cells upon *SLC7A11* knockdown were measured by CellROX-Green flow cytometry assay.

(H) Protein lysates were harvested from the MAPKi-resistant and parental A375 cells with/without *SLC7A11* knockdown. Western blot analysis performed for gamma-H2AX (γH2AX) as a DNA damage marker and cleaved-PARP (cl-PARP) as an apoptosis marker. α-tubulin was used as a loading control.

(I) *SLC7A11* was expressed in parental and MAPKi-resistant A375 cells by lentiviral transduction. pLX304 empty vector was used as the control (ctrl). The level of *SLC7A11* overexpression in parental and MAPKi-resistant cells was measured by qRT-PCR of *SLC7A11* mRNA.

(J and K) Incucyte proliferation assays indicate the responsiveness to 1 μM vorinostat treatment in A375R (J) and A375DR (K) cells with and without *SLC7A11* overexpression.

(L) Long-term colony formation of *SLC7A11*-overexpressing parental and MAPKi-resistant A375 cells in the treatment of vorinostat. The cells were seeded 50,000 cells per well in 6-well plate and cultured 10 days with or without 1 μM vorinostat. Afterward, the cells were fixed, stained, and photographed.

(M) *SLC7A11*-overexpressing parental and MAPKi-resistant A375 cells were treated with 2 μM vorinostat for 72 hr. Afterward, ROS levels were measured using CellROX-Green flow cytometry assay.

Error bars in represent the mean ± SD from the biological triplicates (*p ≤ 0.05, **p ≤ 0.01, ***p ≤ 0.001, Student's t test).

See also Figure S5 and Table S1.

cutaneous T cell lymphoma. Tumor measurements were performed every 8 weeks and tumor tissue was collected for exploratory analyses (Figure 7A). Pharmacokinetics of the drug in patients (Table S3) showed very good concordance with literature data (Iwamoto et al., 2013). Currently, six patients have been treated and an additional 15 patients will be enrolled in this ongoing study. A more detailed report of this trial will be published elsewhere. Relevant to the potential therapeutic application reported above, we present here molecular analyses from three patients (see Table S2 for patient details) from whom we were able to obtain pre-, during, and post-vorinostat treatment biopsies.

Figures 7B–7D show radiological volume measurements of multiple metastatic lesions for these three patients. The curves stop at progression, which is the end of treatment of vorinostat. The time points of biopsies are marked with a red triangle on the

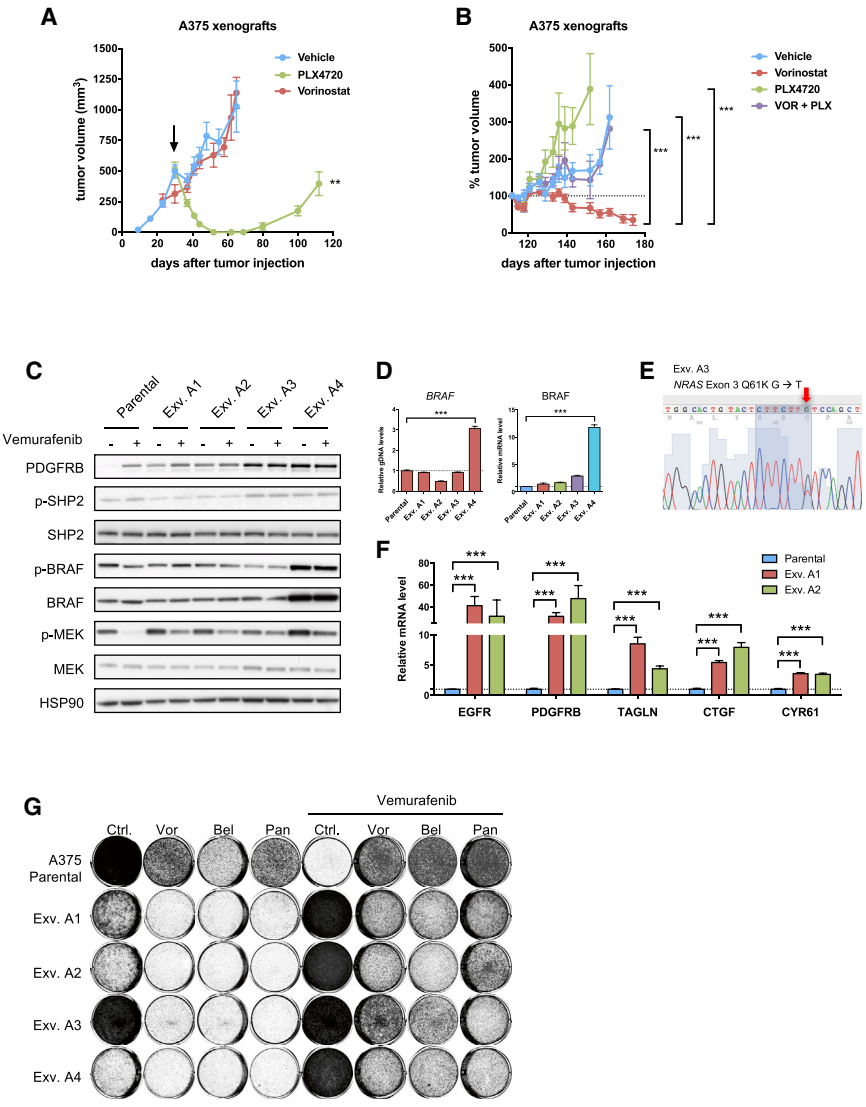

Figure 6. *In Vivo* Responses of *BRAF* Mutant Melanoma to HDAC Inhibitors

(A) Tumor growth of A375 parental cells in the flanks of BALB/c nude mice subcutaneously injected with 1 × 10^6 A375 cells. When tumors reached approximately 500 mm^3 (black arrow), mice were assigned to control chow (n = 8), PLX4720-supplemented chow (40 mg/kg/day, n = 30), or vorinostat (100 mg/kg/day, intraperitoneal injection, n = 5).

(B) On day 112 post-injection, PLX4720-treated mice were assigned to control chow (n = 7), continuous PLX4720-supplemented chow (40 mg/kg/day, n = 6), vorinostat (100 mg/kg/day, intraperitoneal injection, n = 11), or combination PLX4720-supplemented chow (40 mg/kg/day) and vorinostat (100 mg/kg/day, intraperitoneal injection, n = 6).

(C) Four BRAFi-resistant *ex vivo* clones (exv. A1, exv. A2, exv. A3, and exv. A4) were isolated from four different A375 tumors receiving continued PLX4720 treatment from the cohort shown in (B). The protein levels of phosphorylated PDGFRB, p-SHP2, SHP2, p-MEK, MEK, and HSP90 were measured by western blotting, and the A375 parental cell line was treated with 2 μM vemurafenib for 24 hr. HSP90 served as the loading control.

(D) BRAF levels in the four BRAFi-resistant *ex vivo* clones and parental A375 line were determined by qRT-PCR on genomic DNA (left panel) and mRNA (right panel).

(E) Sanger sequencing analysis of NRAS exon 3 in A375 BRAFi-resistant exv. 3 clone.

(F) Fold changes in mean expression levels measured by qRT-PCR of TGFβ target genes *EGFR*, *PDGFRB*, *TAGLN*, *CTGF*, and *CYR61* in A375 BRAFi-resistant exv. 1 and exv. 2 and the A375 parental line.

(G) A375 parental and BRAFi-resistant *ex vivo* clones were treated with a panel of HDACi (1 μM vorinostat, 0.5 μM belinostat, and 6 nM panobinostat) in single treatment or in combination with 1 μM vemurafenib in a long-term colony formation assay.

Error bars represent the mean ± SD from the biological triplicates (*p ≤ 0.05, **p ≤ 0.01, ***p ≤ 0.001, Student's t test).

curve of the lesion from which the biopsy was taken. The red dotted vertical line marks the start of vorinostat therapy. We used the biopsy transcriptome (RNA-seq) data to assess *SLC7A11* levels in these pre-, during, and post-vorinostat-treated tumor biopsies to ask whether HDACi also suppress this gene in patients. Consistent with our *in vitro* data, we observed that vorinostat repressed *SLC7A11* expression in the patient lesions (Figure 7I).

We were particularly interested in whether vorinostat therapy could eradicate tumor cells that had gained resistance to BRAF+MEK inhibitor therapy. To assess this, we isolated DNA from these biopsies and searched for changes in the prevalence of drug resistance mutations in the tumors during vorinostat treatment. Intriguingly, patient A harbored the known MAPKi resistance mutation $KRAS^{G12C}$ before vorinostat treatment at an allele frequency of 44%, but this mutation was reduced to 0% after 3 weeks of vorinostat treatment (Figure 7E). Similarly, the analysis of biopsies from patient B who acquired the $NRAS^{Q61H}$ mutation at 10% allele frequency during the MAPKi treatment was reduced to 0% after vorinostat therapy (Figure 7F). Patient C developed an *NRAS* amplification as judged by the increased read count for the *NRAS* gene and mRNA expression as judged by RNA-seq (Figures 7G and 7H), but its level of amplification and expression was reduced upon vorinostat treatment (Figures 7G and 7H). These findings are in line with our *in vitro* and mouse data and demonstrate that BRAF+MEK inhibitor-resistant melanoma cells can be preferentially eliminated by treatment with vorinostat. No significant effects of vorinostat were seen on infiltration of immune cells in the metastatic lesions (Figure S6).

DISCUSSION

We identify here a vulnerability of *BRAF* mutant melanomas that is specifically acquired upon development of resistance to inhibitors

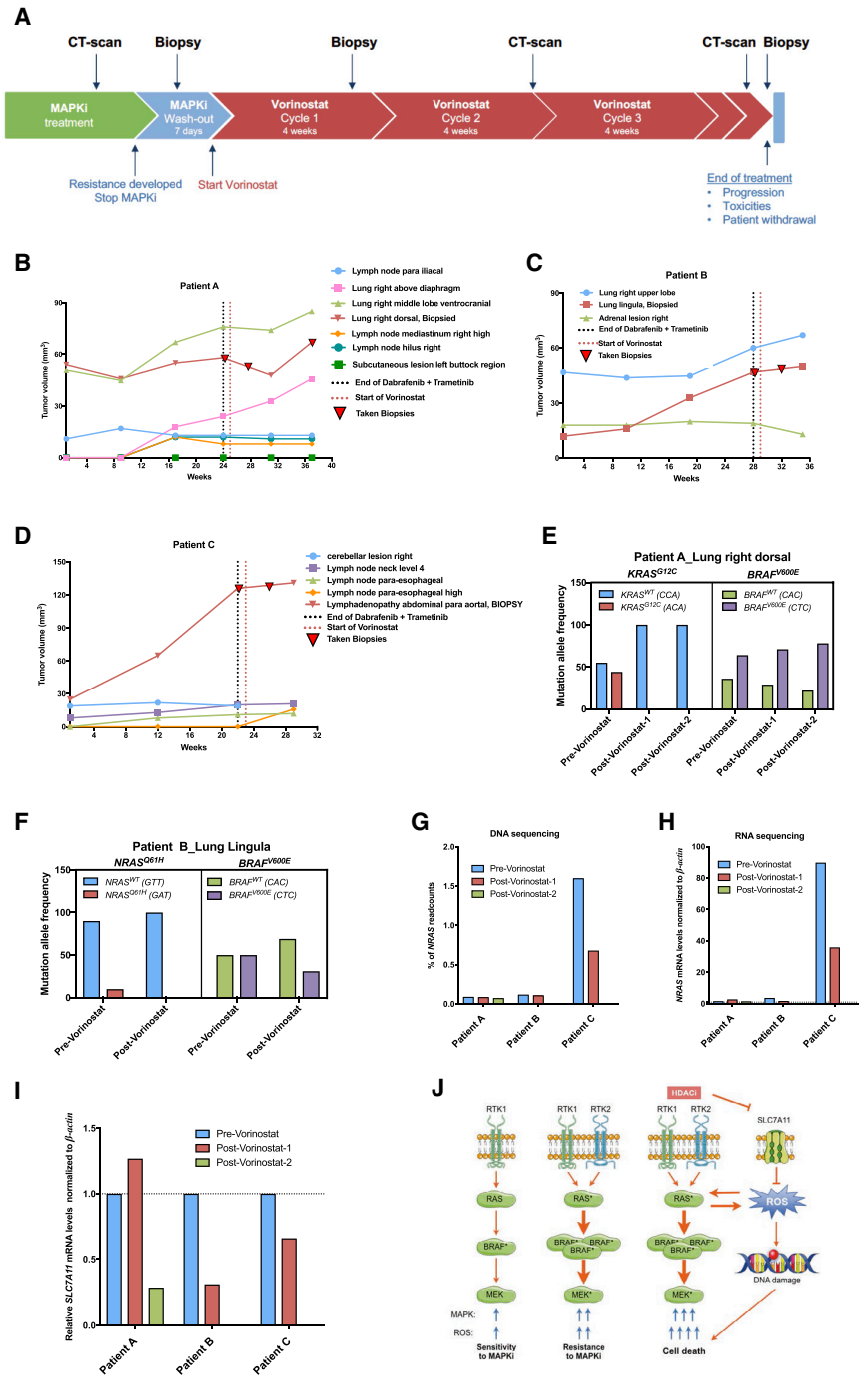

Figure 7. HDACi Responsiveness in MAPK Inhibitor-Resistant Melanoma Patients

(A) Diagram of the design of clinical trial NCT02836548 proof-of-concept study of vorinostat treatment in MAPKi-resistant melanoma patients.

(B) Tumor responsiveness to vorinostat in MAPKi-resistant melanoma patient A evaluated by CT scan measurements. The tumor volume of multiple lesions was plotted on the y axes against time on the x axes.

(C) Like in (B), except for patient B.

(D) Like in (B), except for patient C. Biopsies were collected at indicated time points (inverted red triangles) on the curves of the target lesions (solid red lines).

(E and F) Genomic DNA isolated from the biopsied target lesions of patient A was analyzed using the NKI-178 gene panel using targeted NGS, as described (Groenendijk et al., 2016). Representation of the allele frequency of drug-resistance associated $KRAS^{G12C}$ mutation in patient A (E) and $NRAS^{Q61H}$ in patient B (F) pre- and post-vorinostat treatment. $BRAF^{V600E}$ mutation in each panel served as an indication of tumor cell percentage in the biopsy.

(G) DNA copy number level of *NRAS* gene, as measured by the percentage of NGS reads for this gene as percentage of total captured reads.

(H) Normalized transcript levels of *NRAS* analyzed by RNA-seq in the patients' biopsies pre- and post-vorinostat treatment. β-actin served as a housekeeping gene for normalization.

(I) Fold change in expression levels of *SLC7A11* in patients' biopsies pre- and post-vorinostat treatment deduced from RNA-seq data.

(J) Model for the sequential treatment of melanomas. $BRAF^{V600E}$ (*BRAF**) melanoma cells with normal MAPK signaling and normal ROS levels are sensitive to MAPKi (left). Drug resistance develops through upregulation of RTKs, *RAS* mutations (*RAS**), *BRAF* amplification, or *MEK* mutations (*MEK**), all of which result in enhanced signaling through the MAPK pathway and increased ROS levels (center). Switching therapy from a MAPKi to an HDACi in MAPKi-resistant cells induces ROS through downregulation of *SLC7A11*. The increased ROS also act on RAS to maintain high levels of MAPK signaling. Cellular ROS levels are already increased in MAPKi-resistant tumors, and the further increase of ROS by HDACi leads to a massive DNA damage response that has a lethal effect on the cells (right).

See also Figure S6 and Tables S2 and S3.

of the MAPK pathway. When patients progress on first line therapy, subsequent therapies have a tendency to become increasingly less effective. However, theoretically this does not have to be the case. It is a well-established principle that drug resistance comes at a "fitness cost" for the cancer cell that in turn can lead to novel vulnerabilities of the drug-resistant cells (Hutchison, 1963). Such acquired vulnerabilities have in the past been searched for through compound screens in pairs of sensitive and chemotherapy-resistant cancer cells (Jensen et al., 1997; Rickardson et al., 2006). These efforts have been relatively unproductive from a clinical perspective, most likely because cancer cells have many avenues to become chemotherapy insensitive, making the collateral sensitivities of drug-resistant cells equally heterogeneous and unpredictable. This issue is less relevant for *BRAF* mutant melanoma, as resistance to MAPK pathway inhibition more often than not leads to secondary mutations that reactivate

the MAPK pathway in the presence of drug. This predictable resistance mechanism may also lead to more foreseeable collateral sensitivities as compared to the chemotherapy resistance models. Indeed, our data show that melanoma cells that have acquired resistance to MAPK inhibitors through different MAPK pathway reactivation mechanisms all become sensitive to HDACi, including *PDGFRB* overexpression (A375R cells) (Figure 1C), $NRAS^{Q61H}$ mutation (A375DR cells) (Figure 1D), $KRAS^{G12C}$ (Mel888DR cells) (Figure S1E), *BRAF* splice site mutations (Mel888R cells) (Figure 1D), and *BRAF* amplification (A375 Exv A4) (Figures 6C and 6D). The common vulnerability we identified in these MAPK-resistant cells results from the induction of ROS by hyperactive MAPK pathway signaling. Consequently, further activation of these increased ROS levels by vorinostat leads to significant DNA damage and apoptotic cell death only in the MAPK-resistant cells, but not in the drug-sensitive cells that have lower ROS levels. Consistent with this, we see no effect of vorinostat in MAPK inhibitor-sensitive melanoma cells.

Vorinostat has proven anticancer activity and was approved in 2006 for use in cutaneous T cell lymphoma. Our data indicate that ROS induction plays a major part in the killing of BRAF inhibitor-resistant melanoma cells by vorinostat, as the ROS scavengers NAC and GEE counteracted the vorinostat effects. The vorinostat effect on ROS induction is primarily caused by suppression of *SLC7A11*, as ectopic *SLC7A11* expression rescued ROS induction by vorinostat (Figures 5K and S5G). This gene encodes the importer of cystine, which serves as a precursor to the ROS scavenger glutathione. *SLC7A11* expression did not completely rescue the anti-proliferative effect of vorinostat in BRAF inhibitor-resistant melanoma, consistent with the notion that vorinostat also has ROS-independent effects on cancer cells (Figures 5J and S5F). Together, these data support a model in which the increased ROS level in BRAF-resistant melanoma becomes a liability when ROS levels are increased further by HDACi treatment, leading to DNA damage and apoptotic cell death (Figure 7J).

We find that vorinostat treatment in mouse xenograft tumors that have developed resistance to BRAF inhibitor *in vivo* leads to tumor regression. This was not seen when BRAFi-resistant tumor cells were treated with a combination of BRAFi+HDACi, in agreement with our *in vitro* findings showing that the two drugs are antagonistic. The molecular basis for the notion that BRAFi and HDACi must not be used simultaneously is provided by our finding that increased MAPK signaling resulting from BRAF inhibitor resistance leads to an increase in ROS levels that are increased to toxic levels by subsequent treatment with vorinostat. Conversely, MAPK inhibition with selective drugs diminishes ROS levels. While vorinostat can increase these lower ROS levels in the presence of MAPK inhibitors also, they do not reach toxic concentrations that result in DNA damage and cell death (Figures 3D–3F). The finding that BRAF and HDAC inhibitors must be used sequentially was unexpected as a recent publication demonstrated that combination of BRAF and HDAC inhibitors upfront can prevent emergence of resistant melanoma cells in a short-term assay (Johannessen et al., 2013). This difference most likely has its origin in the notion that the effects of epigenetic drugs like vorinostat take considerable time to develop. That lethal ROS levels can be used to kill cancer cells was recently also shown by others using a combination of mTOR and HDAC inhibitors in *NF1* and *RAS* mutant cancers (Malone et al., 2017). The fundamental difference between this observation and ours is that Malone et al. (2017) used simultaneous treatment with two drugs to increase ROS levels to lethal levels, whereas in our melanoma model, it is mandatory to use the drugs sequentially to reach toxic ROS levels. Indeed, most other recent publications that identify combinations of drugs to prevent resistance development use upfront combinations to accomplish this (Hangauer et al., 2017; Sharma et al., 2010). The sequential treatment we identify here has the advantage that it avoids toxicity arising from simultaneous use of drugs. Therefore, sequential drug therapy enables the clinical use of a much larger drug repertoire than simultaneous use. In a pilot study in patients with advanced *BRAF* mutant melanoma that progressed on BRAF+MEK inhibitor therapy we see that tumor cells harboring a drug-resistance mutation are quickly depleted by vorinostat, consistent with the sensitivity of these cells to vorinostat seen *in vitro* and in mouse models. In patients, tumors initially stabilize upon switch to vorinostat therapy, but then progression occurs. This is not unexpected, given that parental, MAPK inhibitor sensitive, tumor cells fail to respond to vorinostat. After initial depletion of the drug-resistant clones in the tumor by vorinostat therapy, the BRAF+MEK inhibitor sensitive clones continue to proliferate, leading to progression. To avoid this problem, we will adapt the protocol for the ongoing trial NCT02836548 to include monitoring of patients on BRAF+MEK inhibitor therapy for early signs of drug resistance through analysis of cell free tumor DNA in blood (Murtaza et al., 2013). Such mutations are often detectable before radiological progression is evident (Misale et al., 2012). By pulsatile treatment with vorinostat to eradicate emergent drug-resistant cells, followed by a switch back to BRAF+MEK inhibition, we expect to get longer progression free survival benefit for patients as compared to an intermittent BRAF inhibitor only regimen (Das Thakur et al., 2013). Indeed, our *in vitro* data indicate that switching from MAPK inhibitor therapy to vorinostat is more effective in eradicating drug-resistant cells than a drug holiday (Figures 4 and S4). We cannot exclude that drug-resistance mechanisms occur in patients that are not associated with reactivation of the MAPK pathway. If they occur, such drug-resistant variants may not respond to vorinostat therapy. We note that all melanoma cells that acquired resistance *in vitro* or *in vivo*, including the three patients analyzed here, upregulated the MAPK pathway to gain resistance and thereby gained susceptibility to HDAC inhibition. More generally, our data highlight that studying how cancer cells acquire resistance to targeted cancer drugs may be fruitful to identify novel vulnerabilities that can be exploited therapeutically.

STAR★METHODS

Detailed methods are provided in the online version of this paper and include the following:

- KEY RESOURCES TABLE
- CONTACT FOR REAGENT AND RESOURCE SHARING
- EXPERIMENTAL MODEL AND SUBJECT DETAILS
  - Cell lines
  - Mouse xenografts and *in vivo* drug studies
  - Patient studies

- Long-term colony formation assay and IncuCyte cell proliferation assays
- Cell viability measurement
- Protein lysate preparation and immunoblotting
- ROS detection
- Glutathione detection
- Competition assay
- qRT-PCR
- Detection of genomic DNA alterations
- Lentiviral transduction
- Relative growth rate calculation
- Active RAS Pull-Down detection
- Vorinostat synthesis
- NKI 178 gene panel exosome next generation DNA sequencing
- Immunohistochemistry

● QUANTIFICATION AND STATISTICAL ANALYSIS
● DATA AND SOFTWARE AVAILABILITY
● ADDITIONAL RESOURCES

SUPPLEMENTAL INFORMATION

Supplemental Information includes six figures and three tables and can be found with this article online at https://doi.org/10.1016/j.cell.2018.04.012.

ACKNOWLEDGMENTS

We thank Plexxikon (Berkeley, CA, USA) for providing PLX4720. This work was funded by grants from the Dutch Cancer Society (KWF, grant number NKI2012-5401), the European Research Council (ERC, grant number 250043), and the Center for Cancer Genomics (CGC.nl, grant number 024.001.028). The clinical study was supported by a proof of concept ERC grant, grant number 712951.

AUTHOR CONTRIBUTIONS

L.W. and R.L.d.O co-designed the study, performed experiments, and wrote the manuscript. E.B., N.P., D.B., A.B., J.-Y.S., J.Z., G.T.L.-d.V., and H.H. performed and interpreted the experiments. B.N. and J.H.B. synthetized and formulated the vorinostat. S.H. and J.H.M.S. designed and performed the clinical study. R.B. co-designed the study, wrote the manuscript, and supervised the project. All authors contributed to the manuscript text.

DECLARATION OF INTERESTS

L.W., R.L.dO., and R.B. are listed as inventors on a patent application on the use of HDAC inhibitors in MAPKi-resistant melanoma. All other authors declare no competing interests.

Received: October 6, 2017
Revised: February 14, 2018
Accepted: April 11, 2018
Published: May 10, 2018

REFERENCES

Baenke, F., Chaneton, B., Smith, M., Van Den Broek, N., Hogan, K., Tang, H., Viros, A., Martin, M., Galbraith, L., Girotti, M.R., et al. (2016). Resistance to BRAF inhibitors induces glutamine dependency in melanoma cells. Mol. Oncol. *10*, 73–84.

Bannai, S., and Tateishi, N. (1986). Role of membrane transport in metabolism and function of glutathione in mammals. J. Membr. Biol. *89*, 1–8.

Corazao-Rozas, P., Guerreschi, P., Jendoubi, M., André, F., Jonneaux, A., Scalbert, C., Garçon, G., Malet-Martino, M., Balayssac, S., Rocchi, S., et al. (2013). Mitochondrial oxidative stress is the Achilles' heel of melanoma cells resistant to Braf-mutant inhibitor. Oncotarget *4*, 1986–1998.

Das Thakur, M., Salangsang, F., Landman, A.S., Sellers, W.R., Pryer, N.K., Levesque, M.P., Dummer, R., McMahon, M., and Stuart, D.D. (2013). Modelling vemurafenib resistance in melanoma reveals a strategy to forestall drug resistance. Nature *494*, 251–255.

Gout, P.W., Kang, Y.J., Buckley, D.J., Bruchovsky, N., and Buckley, A.R. (1997). Increased cystine uptake capability associated with malignant progression of Nb2 lymphoma cells. Leukemia *11*, 1329–1337.

Groenendijk, F.H., de Jong, J., Fransen van de Putte, E.E., Michaut, M., Schlicker, A., Peters, D., Velds, A., Nieuwland, M., van den Heuvel, M.M., Kerkhoven, R.M., et al. (2016). ERBB2 mutations characterize a subgroup of muscle-invasive bladder cancers with excellent response to neoadjuvant chemotherapy. Eur. Urol. *69*, 384–388.

Hangauer, M.J., Viswanathan, V.S., Ryan, M.J., Bole, D., Eaton, J.K., Matov, A., Galeas, J., Dhruv, H.D., Berens, M.E., Schreiber, S.L., et al. (2017). Drug-tolerant persister cancer cells are vulnerable to GPX4 inhibition. Nature *551*, 247–250.

Haq, R., Shoag, J., Andreu-Perez, P., Yokoyama, S., Edelman, H., Rowe, G.C., Frederick, D.T., Hurley, A.D., Nellore, A., Kung, A.L., et al. (2013). Oncogenic BRAF regulates oxidative metabolism via PGC1α and MITF. Cancer Cell *23*, 302–315.

Hernandez-Davies, J.E., Tran, T.Q., Reid, M.A., Rosales, K.R., Lowman, X.H., Pan, M., Moriceau, G., Yang, Y., Wu, J., Lo, R.S., and Kong, M. (2015). Vemurafenib resistance reprograms melanoma cells towards glutamine dependence. J. Transl. Med. *13*, 210.

Huang, S., Hölzel, M., Knijnenburg, T., Schlicker, A., Roepman, P., McDermott, U., Garnett, M., Grernrum, W., Sun, C., Prahallad, A., et al. (2012). MED12 controls the response to multiple cancer drugs through regulation of TGF-β receptor signaling. Cell *151*, 937–950.

Hutchison, D.J. (1963). Cross resistance and collateral sensitivity studies in cancer chemotherapy. In Advances in Cancer Research, A. Haddow and S. Weinhouse, eds. (Academic Press), pp. 235–350.

Iwamoto, M., Friedman, E.J., Sandhu, P., Agrawal, N.G., Rubin, E.H., and Wagner, J.A. (2013). Clinical pharmacology profile of vorinostat, a histone deacetylase inhibitor. Cancer Chemother. Pharmacol. *72*, 493–508.

Jensen, P.B., Holm, B., Sorensen, M., Christensen, I.J., and Sehested, M. (1997). In vitro cross-resistance and collateral sensitivity in seven resistant small-cell lung cancer cell lines: preclinical identification of suitable drug partners to taxotere, taxol, topotecan and gemcitabin. Br. J. Cancer *75*, 869–877.

Johannessen, C.M., Johnson, L.A., Piccioni, F., Townes, A., Frederick, D.T., Donahue, M.K., Narayan, R., Flaherty, K.T., Wargo, J.A., Root, D.E., and Garraway, L.A. (2013). A melanocyte lineage program confers resistance to MAP kinase pathway inhibition. Nature *504*, 138–142.

Lee, A.C., Fenster, B.E., Ito, H., Takeda, K., Bae, N.S., Hirai, T., Yu, Z.X., Ferrans, V.J., Howard, B.H., and Finkel, T. (1999). Ras proteins induce senescence by altering the intracellular levels of reactive oxygen species. J. Biol. Chem. *274*, 7936–7940.

Mai, A., Esposito, M., Sbardella, G., and Massa, S. (2001). A new facile and expeditious synthesis of n-hydroxy-n'-phenyloctanediamide, a potent inducer of terminal cyclodifferentiation. Org Prep Proced Int *33*, 391–394.

Malone, C.F., Emerson, C., Ingraham, R., Barbosa, W., Guerra, S., Yoon, H., Liu, L.L., Michor, F., Haigis, M., Macleod, K.F., et al. (2017). mTOR and HDAC inhibitors converge on the TXNIP/thioredoxin pathway to cause catastrophic oxidative stress and regression of RAS-driven tumors. Cancer Discov. *7*, 1450–1463.

Manzano, J.L., Layos, L., Bugés, C., de Los Llanos Gil, M., Vila, L., Martínez-Balibrea, E., and Martínez-Cardús, A. (2016). Resistant mechanisms to BRAF inhibitors in melanoma. Ann. Transl. Med. *4*, 237.

Misale, S., Yaeger, R., Hobor, S., Scala, E., Janakiraman, M., Liska, D., Valtorta, E., Schiavo, R., Buscarino, M., Siravegna, G., et al. (2012). Emergence

of KRAS mutations and acquired resistance to anti-EGFR therapy in colorectal cancer. Nature *486*, 532–536.

Murtaza, M., Dawson, S.J., Tsui, D.W., Gale, D., Forshew, T., Piskorz, A.M., Parkinson, C., Chin, S.F., Kingsbury, Z., Wong, A.S., et al. (2013). Non-invasive analysis of acquired resistance to cancer therapy by sequencing of plasma DNA. Nature *497*, 108–112.

Petruccelli, L.A., Dupéré-Richer, D., Pettersson, F., Retrouvey, H., Skoulikas, S., and Miller, W.H., Jr. (2011). Vorinostat induces reactive oxygen species and DNA damage in acute myeloid leukemia cells. PLoS ONE *6*, e20987.

Reczek, C.R., and Chandel, N.S. (2017). The two faces of reactive oxygen species in cancer. Annu. Rev. Cancer Biol. *1*, 79–98.

Rickardson, L., Fryknäs, M., Haglund, C., Lövborg, H., Nygren, P., Gustafsson, M.G., Isaksson, A., and Larsson, R. (2006). Screening of an annotated compound library for drug activity in a resistant myeloma cell line. Cancer Chemother. Pharmacol. *58*, 749–758.

Robert, C., Karaszewska, B., Schachter, J., Rutkowski, P., Mackiewicz, A., Stroiakovski, D., Lichinitser, M., Dummer, R., Grange, F., Mortier, L., et al. (2015). Improved overall survival in melanoma with combined dabrafenib and trametinib. N. Engl. J. Med. *372*, 30–39.

Ruefli, A.A., Ausserlechner, M.J., Bernhard, D., Sutton, V.R., Tainton, K.M., Kofler, R., Smyth, M.J., and Johnstone, R.W. (2001). The histone deacetylase inhibitor and chemotherapeutic agent suberoylanilide hydroxamic acid (SAHA) induces a cell-death pathway characterized by cleavage of Bid and production of reactive oxygen species. Proc. Natl. Acad. Sci. USA *98*, 10833–10838.

Seghers, A.C., Wilgenhof, S., Lebbé, C., and Neyns, B. (2012). Successful rechallenge in two patients with BRAF-V600-mutant melanoma who experienced previous progression during treatment with a selective BRAF inhibitor. Melanoma Res. *22*, 466–472.

Sharma, S.V., Lee, D.Y., Li, B., Quinlan, M.P., Takahashi, F., Maheswaran, S., McDermott, U., Azizian, N., Zou, L., Fischbach, M.A., et al. (2010). A chromatin-mediated reversible drug-tolerant state in cancer cell subpopulations. Cell *141*, 69–80.

Son, Y., Cheong, Y.K., Kim, N.H., Chung, H.T., Kang, D.G., and Pae, H.O. (2011). Mitogen-activated protein kinases and reactive oxygen species: how can ROS activate MAPK pathways? J. Signal Transduct. *2011*, 792639.

Sosman, J.A., Kim, K.B., Schuchter, L., Gonzalez, R., Pavlick, A.C., Weber, J.S., McArthur, G.A., Hutson, T.E., Moschos, S.J., Flaherty, K.T., et al. (2012). Survival in BRAF V600-mutant advanced melanoma treated with vemurafenib. N. Engl. J. Med. *366*, 707–714.

Sun, C., Wang, L., Huang, S., Heynen, G.J.J.E., Prahallad, A., Robert, C., Haanen, J., Blank, C., Wesseling, J., Willems, S.M., et al. (2014). Reversible and adaptive resistance to BRAF(V600E) inhibition in melanoma. Nature *508*, 118–122.

Ungerstedt, J.S., Sowa, Y., Xu, W.S., Shao, Y., Dokmanovic, M., Perez, G., Ngo, L., Holmgren, A., Jiang, X., and Marks, P.A. (2005). Role of thioredoxin in the response of normal and transformed cells to histone deacetylase inhibitors. Proc. Natl. Acad. Sci. USA *102*, 673–678.

Valko, M., Leibfritz, D., Moncol, J., Cronin, M.T., Mazur, M., and Telser, J. (2007). Free radicals and antioxidants in normal physiological functions and human disease. Int. J. Biochem. Cell Biol. *39*, 44–84.

Van Allen, E.M., Wagle, N., Sucker, A., Treacy, D.J., Johannessen, C.M., Goetz, E.M., Place, C.S., Taylor-Weiner, A., Whittaker, S., Kryukov, G.V., et al.; Dermatologic Cooperative Oncology Group of Germany (DeCOG) (2014). The genetic landscape of clinical resistance to RAF inhibition in metastatic melanoma. Cancer Discov. *4*, 94–109.

Vazquez, F., Lim, J.H., Chim, H., Bhalla, K., Girnun, G., Pierce, K., Clish, C.B., Granter, S.R., Widlund, H.R., Spiegelman, B.M., and Puigserver, P. (2013). PGC1α expression defines a subset of human melanoma tumors with increased mitochondrial capacity and resistance to oxidative stress. Cancer Cell *23*, 287–301.

Wagle, N., Van Allen, E.M., Treacy, D.J., Frederick, D.T., Cooper, Z.A., Taylor-Weiner, A., Rosenberg, M., Goetz, E.M., Sullivan, R.J., Farlow, D.N., et al. (2014). MAP kinase pathway alterations in BRAF-mutant melanoma patients with acquired resistance to combined RAF/MEK inhibition. Cancer Discov. *4*, 61–68.

Wolf, I.M., Fan, Z., Rauh, M., Seufert, S., Hore, N., Buchfelder, M., Savaskan, N.E., and Eyüpoglu, I.Y. (2014). Histone deacetylases inhibition by SAHA/vorinostat normalizes the glioma microenvironment via xCT equilibration. Sci. Rep. *4*, 6226.

STAR★METHODS

KEY RESOURCES TABLE

REAGENT or RESOURCE	SOURCE	IDENTIFIER
Antibodies		
HSP 90 (H-114), Rabbit polyclonal antibody	Santa Cruz Biotechnology	Cat#: sc-7947; RRID: AB_2121235
Vinculin / VINC, Mouse monoclonal antibody	Sigma-Aldrich	Cat#: V9131; RRID: AB_477629
α-tubulin (CP06), Mouse monoclonal antibody	Millipore	Cat#: CP06; RRID: AB_2617116
β-actin (C-2), Mouse monoclonal antibody	Santa Cruz Biotechnology	Cat#: sc-8432; RRID: AB_626630
Histone 3 / H3, Rabbit polyclonal antibody	Cell Signaling Technology	Cat#: 9715; RRID: AB_331563
acetyl-Histone 3 / ac-H3, Rabbit polyclonal antibody	Millipore	Cat#: 06-599; RRID: AB_2115283
Phospho-Rb (Ser780), Rabbit polyclonal antibody	Cell Signaling Technology	Cat#: 39033; RRID:AB_330015
Phospho-MEK1/2 (Ser217/221) (41G9), Rabbit monoclonal antibody	Cell Signaling Technology	Cat#: 9154S; RRID: AB_2138017
MEK1/2 (L38C12), Mouse monoclonal antibody	Cell Signaling Technology	Cat#: 4694S; RRID: AB_10695868
SHP2 (C-18), Rabbit polyclonal antibody	Santa Cruz Biotechnology	Cat#: SC-280; RRID: AB_632401
p-SHP2, Rabbit monoclonal antibody	Abcam	Cat#: ab62322; RRID: AB_945452
Pan-Ras (Ras10), Mouse monoclonal antibody	Thermo Scientific	Cat#: MA1-012X; RRID: AB_2536665
PDGFRB (C82A3), Rabbit monoclonal antibody	Cell Signaling Technology	Cat#: 4564; RRID: AB_2236927
p-BRAF (Ser445), Rabbit polyclonal antibody	Cell Signaling Technology	Cat#: #2696; RRID: AB_390721
BRAF (F-7), Mouse monoclonal antibody	Santa Cruz Biotechnology	Cat#: sc-5284; RRID: AB_626760
Cleaved PARP (Asp214) (D64E10) XP, Rabbit monoclonal antibody	Cell Signaling Technology	Cat#: #5625; RRID: AB_10699459
phospho-Rsk1 (Thr359/Ser363), Rabbit monoclonal antibody	Millipore	Cat#: 04-419; RRID: AB_11213444
RSK1 (D6D5), Rabbit monoclonal antibody	Cell Signaling Technology	Cat#: 8408S; RRID: AB_10828594
γH2AX, Mouse monoclonal antibody	Millipore	Cat # 05-636; RRID: AB_309864
CD3 (SP7) for IHC, Rabbit monoclonal antibody	Spring Bioscience	Cat # M3071; RRID: 1660770
CD4 (SP35) for IHC, Rabbit monoclonal antibody	Cell Marque	Cat # 104R-14; RRID: 1516770
CD8 (C8/144B) for IHC, Mouse monoclonal antibody	Dako/Agilent	Cat # M7103; RRID: 2075537
CD20 (L26) for IHC, Mouse monoclonal antibody	Dako/Agilent	Cat # N/A; RRID: N/A
CD68 (KP1) for IHC, Mouse monoclonal antibody	Dako/Agilent	Cat # GA60961-2; RRID: 2661840
Chemicals, Peptides, and Recombinant Proteins		
Vorinostat	Selleck Chemicals	Cat#: S1047
Dabrafenib	Selleck Chemicals	Cat#: S2807
Trametinib	Selleck Chemicals	Cat#: S2673
Vemurafenib	Selleck Chemicals	Cat#: S1267
Entinostat	Selleck Chemicals	Cat#: S1053
Panobinostat	Selleck Chemicals	Cat#: S1030
Belinostat	Selleck Chemicals	Cat#: S1085
Paraquat	Sigma-Aldrich	Cat#: 36541
N-Acetyl-L-cysteine (NAC)	Sigma-Aldrich	Cat#: A0150000
tert-Butyl hydroperoxide	Sigma-Aldrich	Cat#: 416665
Vorinostat (used in *in vivo*)	LC Laboratories	Cat#: V-8477
Vorinostat (used in clinic)	Synthesized by J. Beijnen	N/A

(*Continued on next page*)

Continued

REAGENT or RESOURCE	SOURCE	IDENTIFIER
PLX4720 chow	Produced by Research Diets Inc PLX4720 was provided by Plexxikon	N/A
Glutathione reduced ethyl ester (GEE)	Sigma-Aldrich	Cat#: G1404
6-Hydroxy-2,5,7,8-tetramethylchromane-2-carboxylic acid (Trolox)	Sigma-Aldrich	238813-1G
Critical Commercial Assays		
RAF-1 RBD Agarose	Merck Millipore	Cat#: 14-278
FastStart Universal SYBR Green Master (Rox)	Roche	Cat#: 04913850001
Quick-RNA MiniPrep	Zymo Research	Cat#: R1055
CellTiter-Blue Cell Viability Assay	Promega	Cat#: G8081
Maxima First Strand cDNA Synthesis Kit for RT-qPCR	Thermo Fisher	Cat#: K1641
Glutathione detection kit	Enzo	Cat#: ADI-900-160
CellROX Green Flow Cytometry Assay Kit	Life Technologies	Cat#: C10492
Deposited Data		
NKI 178-gene panel exosome DNA sequencing from tumor biopsies	NKI-AVL, The Genomics Core Facility	GSE 111140
RNA sequencing data from Cell line and tumor biopsies	NKI-AVL, The Genomics Core Facility	GSE 110948
Experimental Models: Cell Lines		
A375	ATCC	RRID:CVCL_0132 (Female cell line)
SK-MEL-2	ATCC	RRID: CVCL_0069 (Female cell line)
SK-MEL-147	ATCC	RRID:CVCL_3876 (Gender undefined)
Colo741	R. Marais (Manchester, UK)	RRID:CVCL_1133 (Female cell line)
Mel888	D. Peeper (NKI, Amsterdam, the Netherlands)	RRID:CVCL_4632 (Female cell line)
A375 *ex vivo* BRAFi-resistant clones	This paper	(Female cell line)
Experimental Models: Organisms/Strains		
Clinic study	Registered under ClinicalTrials.org	NCT02836548
Patient information	This paper	Table S2
Recombinant DNA		
pLKO 0.1 (TRC)	Sigma-Aldrich TRC shRNA collection	N/A
pLKO-shSLC7A11 shRNAs	K. Lint (NKI, Amsterdam, the Netherlands)	N/A
pLKO-H2A-GFP	K. Lint (NKI, Amsterdam, the Netherlands)	N/A
pLKO-H2A-RFP	Addgene	Cat#: #25890
pLX304-empty	SSCB Broad ORF lentiviral expression collection	N/A
pLX304-SLC7A11	N/A	N/A
Sequence-Based Reagents		
shRNA target sequences	Sigma-Aldrich TRC shRNA collection	TRCN0000043123
shSLC7A11#1: CCGGCCTGTCACTATTTGGAGCTTTCTCGA GAAAGCTCCAAATAGTGACAGGTTTTTG	Sigma-Aldrich TRC shRNA collection	TRCN0000043127

(*Continued on next page*)

Continued

REAGENT or RESOURCE	SOURCE	IDENTIFIER
shSLC7A11#2: CCGGGCTGATTTATCTTCGATACAACTCGAG TTGTATCGAAGATAAATCAGCTTTTTG	Sigma-Aldrich TRC shRNA collection	TRCN0000288865
shSLC7A11#3: CCGGCCTGCGTATTATCTCTTTATTCTCGAG AATAAAGAGATAATACGCAGGTTTTTG	Sigma-Aldrich TRC shRNA collection	TRCN0000380471
shSLC7A11#4: GTACCGGCCCTCTATTCGGACCCATTTACTCGAGTAAATGGGT CCGAATAGAGGGTTTTTTG	N/A	N/A
gGAPDH Forward: 5′-CCACCCAGAAGACTGTGGAT-3′	Invitrogen	N/A
gGAPDH Reverse: 5′-TTCAGCTCAGGGATGACCTT-3′	Invitrogen	N/A
gNRAS exon3 Forward: 5′-TGGCAAATACACAGAGGAAGC-3′	Invitrogen	N/A
gNRAS exon3 Reverse: 5′-CACACCCCCAGGATTCTTAC-3′	Invitrogen	N/A
gKRAS exon2 Forward: 5′-AGAATGGTCCTGCACCAGTAA-3′	Invitrogen	N/A
gKRAS exon2 Reverse: 5′-TTAACCTTATGTGTGACATGT TCTAA-3′	Invitrogen	N/A
gBRAF Forward: 5′- CAAGTCACCACAAAAACCTATCGT-3′	Invitrogen	N/A
gBRAFReverse: 5′- AACTGACTCACCACTGTCCTCTGTT-3′	Invitrogen	N/A
GAPDH Forward: 5′-AAGGTGAAGGTCGGAGTCAA-3′	Invitrogen	N/A
GAPDH Reverse: 5′-AATGAAGGGGTCATTGATGG-3′	Invitrogen	N/A
PDGFRB Forward: 5′- CAGGAGAGACAGCAACAGCA-3′	Invitrogen	N/A
PDGFRB Reverse: 5′- TGTCCAGAGCCTGGAACTGT-3′	Invitrogen	N/A
EGFR Forward: 5′-TCCTCTGGAGGCTGAGAAAA-3′	Invitrogen	N/A
EGFR Reverse: 5′-GGGCTCTGGAGGAAAAGAAA-3′	Invitrogen	N/A
TAGLN Forward: 5′-GTCCGAACCCAGACACAAGT-3′	Invitrogen	N/A
TAGLN Reverse: 5′- CTCATGCCATAGGAAGGACC-3′	Invitrogen	N/A
CYR61 Reverse: 5′- GCTGGAATGCAACTTCGG-3′	Invitrogen	N/A
CYR61 Forward: 5′-CCCGTTTTGGTAGATTCTGG-3′	Invitrogen	N/A
CTGF Reverse: 5′-TACCAATGACAACGCCTCCT-3′	Invitrogen	N/A
CTGF Reverse: 5′- TGGAGATTTTGGGAGTACGG-3′	Invitrogen	N/A
BRAF Forward: 5′-GTGGATTATGCTCCCCACC-3′	Invitrogen	NA
BRAF Reverse: 5′-CTGCCATTCCGGAGGAG-3′	Invitrogen	N/A
SLC7A11 Forward: 5′-AGCACATAGCCAATGGTGAC-3′	Invitrogen	N/A
SLC7A11 Reverse: 5′- GCTGGCTGGTTTTACCTCAA-3′	Invitrogen	N/A
Software and Algorithms		
Prism version 7.0	GraphPad Software	N/A
FlowJo version 7.6.5	FlowJo, LLC	N/A
qPrimerDepot		N/A
IncuCyte ZOOM system	ESSEN Bioscience	N/A
4 Peaks version 1.7.2	Nucleobytes	N/A
IGV verison 2.3.61 (88)	Broad Institute	N/A

CONTACT FOR REAGENT AND RESOURCE SHARING

Further information and requests for resources and reagents should be directed to and will be fulfilled by the Lead Contact, Rene Bernards (r.bernards@nki.nl).

EXPERIMENTAL MODEL AND SUBJECT DETAILS

Cell lines

The A375, SK-MEL-2 and SK-MEL-147 melanoma cell line was obtained from ATCC. Mel888 cells were gifts from D. Peeper (Amsterdam, the Netherlands). Colo741 cell lines were provided by R. Marais (Manchester, UK). All the cell lines were cultured in a DMEM-based medium supplemented with 10% FBS, 1% penicillin/streptomycin and 2 mM L-glutamine. Vemurafenib-resistant A375R, Mel888R were generated by long term (at least 3 months) culturing with 2 μM vemurafenib. Dabrafenib-trametinib double-resistant A375DR and Mel888DR were generated by long term (at least 3 months) culturing with 0.25 μM dabrafenib and 10nM trametinib. Vemurafenib-resistant *ex vivo* clones were isolated from immunodeficient BalbC mice, which were engrafted with A375 and long-term treated with PLX4720-supplemented chow (40mg/kg). All the *in vitro* cell lines have been validated by STR profiling and regularly tested for Mycoplasma spp with PCR-based assay.

Mouse xenografts and *in vivo* drug studies

All animal experiments were approved by the Animal Ethics Committee of the Netherlands Cancer Institute and performed in accordance with institutional, national and European guidelines for Animal Care and Use. Two million A375 *BRAF*(*V600E*) melanoma cells were resuspended in PBS were mixed 1:1 with matrigel and injected subcutaneously into the posterior flanks of 7-week-old immunodeficient BalbC nude female mice (6 mice per group; Janvier Laboratories, the Netherlands). Tumor formation was monitored twice a week, and tumor volume based on calliper measurements was calculated by the modified ellipsoidal formula (tumor volume = 1/2(length × width^2)). When tumors reached a volume of approximately 0.5 cm^3, mice were randomized into two treatment arms (Phase I): BRAF inhibitor PLX4720 (Plexxikon) formulated in the chow dosed at 40 mg/kg (Research Diets Inc) or normal chow. Upon BRAFi resistance emergence in the group treated with PLX4720, mice bearing tumors of approximately 0.3 cm^3 were once again randomized into the following treatment arms (Phase II): no drug, vorinostat only, PLX4720 only or the combination of vorinostat and PLX4720. Vorinostat was formulated in DMSO: Kolliphor EL (#27963, Sigma-Aldrich): Saline solution, with the ratio of (1:1:8), and it was dosed at 100 mg/kg daily by intraperitoneal injection.

Patient studies

Each patient being considered for the study received detailed information on the study procedures, the experimental treatment, the potential risks and benefits of the treatment, possible standard treatment alternatives, and the fundamental rights of a patient included in an experimental study/clinical trial, fully compliant with the Helsinki declaration (https://www.wma.net/en/30publications/10policies/b3/). Patient Information Sheets (PIS, also called Informed Consent) were provided to all participants in the study. The information was provided by a physician in charge of the trial, and an informed consent document approved by the Ethics Committee, were given to the patient. Patients were provided with sufficient time to consider all aspects of the trial and associated translational studies. Written informed consent was obtained of every participating subject prior to their registration into the trial. The study was approved by Medical Ethics Committee (METC) of the Antoni van Leeuwenhoek Hospital. Patient A: 58-year-old female, melanoma stage IV. Patient B: 48-year-old male, melanoma stage IV, Patient C: 54-year-old male, melanoma stage IV.

Long-term colony formation assay and IncuCyte cell proliferation assays

Cells were seeded into 6-well plates (50,000 cells per well) or 12-well plates (30,000 cells per well) and cultured both in the absence and presence of drugs as indicated for 10-15 days. At the end of the assay, cells were fixed with 4% of *formaldehyde* (#1.04002, Millipore) diluted in PBS, stained with 2% of crystal violet (#HT90132 Sigma-Aldrich) diluted in water and photographed. For IncuCyte proliferation assays, cells were seeded in 384-well plate (400 cells per well) and cultured in absence or presence of drugs as indicated. Cell confluence was measured and quantified by the IncuCyte imaging system (Essen Bioscience).

Cell viability measurement

Cell viability was detected using CellTiter-Blue Cell Viability Assay Kit (G8081, Promega) according to the manufacturer's instructions. The assay measurement was performed using EnVision multi-label plate reader (PerkinElmer).

Protein lysate preparation and immunoblotting

Cells were seeded in DMEM-based medium containing 10% fetal bovine serum (FBS) in the absence or presence of drug for 48 or 72 hr. The drugs were daily refreshed. Afterward, the cells were washed with PBS and lysed with RIPA buffer supplemented with protease inhibitors (cOmplete, Roche) and phosphatase inhibitor cocktails II and III (Sigma). All lysates were freshly prepared and processed with Novex NuPAGE Gel Electrophoresis Systems (Invitrogen). The detection was performed after 48 or 72 hr drug treatment.

ROS detection

The cells were treated in the absence or presence of drugs for 72 hr, daily refreshed. ROS level in cells was detected using CellROX Green Flow Cytometry Assay Kit (C10492, Life Technologies) according to the manufacturer's instructions. Drugs remained present during the assay.

Glutathione detection

The cells were treated in the absence or presence of drugs for 72 hr, daily refreshed. Total GSH level in cells was detected using Glutathione detection kit (ADI-900-160, Enzo) according to the manufacturer's instructions.

Competition assay

The MAPKi-resistant cells were stably transfected with pLKO-H2B-RFP. The MAPKi-sensitive parental cells were stably transfected with pLKO-H2B-GFP. Afterward, two cell populations were mixed and then seeded 2,000,000 cells into 10-cm dishes for biological replicates and different 6 treatment arms. At each time point, the distribution of the cell populations was determined using flow cytometry (The BD LSRFortessa cell analyzer, BD Biosciences). The ratio of two cell populations was indicated. Day 0 is the starting of the assay; this also indicates the ratio of the seeded GFP and RFP cells. The medium containing drugs were refreshed during each time point. During the experiment, when cells reach 80% confluency in the plates, the cells were re-seeded 2,000,000 cells into a new 10-cm dish.

qRT-PCR

Total RNA was extracted from cells using TRIzol reagent from Invitrogen or Quick-RNA MiniPrep (# R1055) from Zymo Research. cDNA synthesis was performed using Maxima Universal First Strand cDNA Synthesis Kit (#K1661) from Thermo scientific. qPCR reactions were performed with FastStart Universal SYBR Green Master (Rox) from Roche. The experiments were performed according to the manufacturer's instructions. The sequences of the primers used for qRT–PCR analyses are described in the Key Resources Table. All reactions were run in triplicate. The CT values were calculated using the Standard Curve Method.

Detection of genomic DNA alterations

Genomic DNA was isolated using DNeasy Blood&Tissue kit (#6950, QIAGEN) according to the manufacturer's instructions. 40ng gDNA was inputted for 40 cycles of PCR. Next, the PCR products were cleaned with ExoSAP-IT (#78200**,** Affymetrix) and capillary sequenced using the BigDye terminator V3.1 sequencing Kit (Applied Biosystems). The sequences of the primers used to detect the genomic alternations in NRAS, KRAS and BRAF are described in Table S1. All the sequencing was verified with Forward and Reverse primers.

Lentiviral transduction

A third-generation lentivirus packaging system consisting of pCMV-VSV-G (addgene#8454), pRSV-Rev (Addgene#12253) and pMDLg/pRRE (Addgene#12251) was used to create virus particles of the modified reporter plasmids. A transient transfection was performed in 293T cells and lentiviral supernatants were produced. Destination cells were infected with lentiviral supernatants, using 8 μg/ml Polybrene and low virus titer. After 48h of incubation, the supernatant was replaced by medium containing 10 μg/ml Blasticidin or 2 μg/ml Puromycin. After 48h, selection of viral transduced cell lines was completed. All the lentiviral vectors in the study are described in supplemental experiment procedure.

Relative growth rate calculation

The growth rate of each replicate was calculated as the slope a curve fitted through the linear range of the log-transformed confluence measurements (the first 84 hr for A375R and 76 hr for A375DR) of the Incucyte proliferation experiment. For each cell line, the growth rates were normalized to the mean of the untreated controls. The growth rate of untreated control was considered as a basal line and normalized to 1. The relative growth rates of all growth rates of the drug-treated and genetic manipulated arms were compared with the untreated control arm. Error bars indicate standard deviation of 4 replicates.

Active RAS Pull-Down detection

Melanoma cells were treated in the absence or presence of drugs for 72 hr, daily refreshed. RAS-GTP levels were detected using RAS Assay Reagent (RAF-1 RBD, agarose, Merck Millipore according to the manufacturer's instructions.

Vorinostat synthesis

Vorinostat (N-hydroxy-N'-phenyloctanediamide) has been synthesized with suberic acid as starting material. The method is based on the procedure described by Mai et al. (2001). Suberic acid was treated with acetic anhydride to form its cyclic anhydride. By stirring in tert- butylmethylether rather pure cyclized anhydride is obtained. The second step is the reaction of the cyclized anhydride with aniline. This yields three products: suberic acid, mono-anilide (desired product) and bis-anilide. The mono-anilide is isolated in relatively high purity from the mixture. A final trituration in tert-butylmethylether will give 93%–96% pure mono-anilide. Last step is the formation of the hydroxylamide to form vorinostat. After multiple crystalizations the desired purity of 99% is obtained. All conversions, after each step, are followed by ^{1}H NMR spectroscopy and liquid chromatography with mass spectrometric (LC-MS) detection. Vorinostat capsules have been manufactured under GMP conditions by mixing vorinostat drug substance with microcrystalline cellulose PH102 followed by semi-automatic filling into red, hard gelatin capsules (size 0). Each capsule contains an amount of 90 mg vorinostat. Vorinostat capsules are packed per 28 capsules in HD-PE containers and labeled according to GMP EU Annex 13. Vorinostat capsules are stable for at least 1 year at room temperature. Quality control of vorinostat capsules encompasses determination of identity,

content, purity, and uniformity of dosage units, using a validated reversed phase high performance liquid chromatography method with UV detection at 241 nm. Column: Symmetry Shield RP8 150 × 2.1 mm ID and particle size 3.5 μm. Mobile phase: A, 0.5% acetic acid in water; B, 0.5% acetic acid in acetonitrile (90/10). Flow: 300 μL/min. Temperature: 30°C.

NKI 178 gene panel exosome next generation DNA sequencing

DNA were isolated from the fresh frozen tumor biopsies. Target enrichment DNA next-generation sequencing was performed with a custom SureSelect XT2 bait library (Agilent Technologies) covering a selected panel of 178 genes, consisting of (indirect or direct) clinically relevant genes. The experimental details are described (Groenendijk et al., 2016).

Immunohistochemistry

Immunohistochemistry of the FFPE tumor samples was performed on a BenchMark Ultra (CD3, CD4, CD8, CD20, CD56 and CD68) automated stainer (Ventana Medical Systems). Briefly, paraffin sections were cut at 3 um, heated at 75°C for 28 min and deparaffinized in the instrument with EZ prep solution (Ventana Medical Systems). Heat-induced antigen retrieval was carried out using Cell Conditioning 1 (CC1, Ventana Medical Systems) for 32 min at 95°C (CD3, CD4, CD8, CD20, CD56 and CD68). CD3 was detected using clone SP7 (1/100 dilution, 32 min at 37°C, Spring / ITK), CD4 clone SP35 (1/50 dilution, 32 min at 37°C, Cell Marque), CD8 clone C8/144B (Dako / Agilent) using 1/200 dilution 32 min at 37°C, CD20 using clone L26 (1/800 dilution, 32 min at 37°C, Dako / Agilent), CD56 clone MRQ-75 (1/2000 dilution, 32 min at 37°C, Cell Marque), CD68 clone KP1 (Dako / Agilent) using 1/20000 dilution 32 min at 37°C. detection for CD markers were visualized using the OptiView DAB Detection Kit (Ventana Medical Systems). Slides were counterstained with Hematoxylin and Bluing Reagent (Ventana Medical Systems).

QUANTIFICATION AND STATISTICAL ANALYSIS

Statistical significance was calculated by Student's t test with two tails. Prism and Microsoft Excel were used to generate graphs and statistical analyses. *p value < 0.05, **p value < 0.01, ***p value < 0.001. For animal experiments, no statistics methods were used to predetermine sample size; we used the generally accepted number of tumors per treatment group.

DATA AND SOFTWARE AVAILABILITY

Raw and processed data from the next generation RNA sequencing of patient biopsies before and after therapy with HDAC inhibitors have been deposited to NCBI Gene Expression Omnibus (GEO) under accession number GSE110948. DNA sequencing of the patient samples is deposited under accession number GSE111140.

ADDITIONAL RESOURCES

The clinical study described in this manuscript was registered under number NCT02836548 and can be accessed at https://clinicaltrials.gov/show/NCT02836548.

Cell

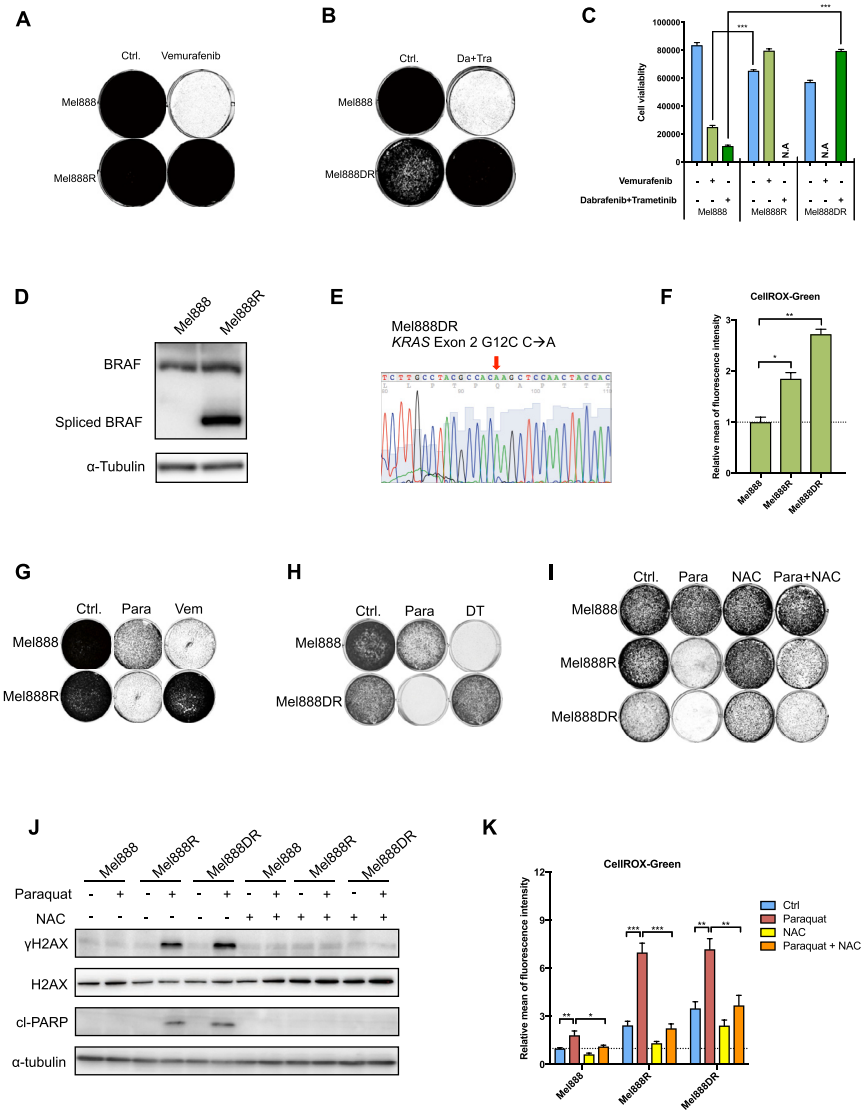

Figure S1. ROS Levels and ROS Sensitivity of Additional Melanoma Cells, Related to Figure 1

(A) Long-term colony formation assay of parental (Mel888) and BRAFi-resistant (Mel888R) melanoma cells were seeded 50,000 cells per well in a 6-well plate and cultured in the presence or absence of 2 μM vemurafenib for 10 days.

(B) Long-term colony formation assay of parental (Mel888) and BRAFi/MEKi-double drug resistant (Mel888DR) melanoma cells were seeded 50,000 cells per well in a 6-well plate and cultured in the presence or absence of 0.5 μM dabrafenib and 10 nM trametinib.

(C) Cell viability assay of parental and drug-resistant cells were seeded 3,000 cells per well in a 96-well plate and cultured in the presence or absence of MAPK inhibitors for 96 hr, and then measured with CellTiter-Blue.

(D) Protein western blot analysis for BRAF indicating that Mel888R cells harbor a 61 kDa *BRAF* variant.

(E) Sanger sequencing of the *KRAS* gene in Mel888DR cells showing a $KRAS^{G12C}$ mutation.

(F) ROS levels of Mel888R, Mel888DR and their parental cells were measured after 72 hr culturing without drugs. ROS levels were measured using CellROX-Green flow cytometry assay. Relative ROS inductions are plotted.

(G and H) Long-term colony formation assay of Mel888R (G), Mel888DR (H) and their parental cells in the treatment of paraquat and/or MAPK inhibitors. Cells were seeded 50,000 cells per well in 6-well plates and treated with 20 μM paraquat, 2 μM vemurafenib or combination of 10nM trametinib and 0.5 μM dabrafenib for 10 days. Afterward, the cells were fixed, stained, and photographed.

(I) Long-term colony formation assays of parental and MAPKi-resistant Mel888 cells in the treatment of paraquat and/or NAC. Cells were seeded 50,000 cells per well in 6-well plates and treated with 20 μM paraquat and/or 2.5 mM N-acetylcysteine (NAC) for 10 days. Afterward, the cells were fixed, stained, and photographed.

(J) Protein lysates were harvest from the MAPKi-resistant (R and DR) and parental Mel888 cells treated with 25 μM paraquat and/or 2.5mM NAC for 72 hr. Western blot analysis showing γH2AX as a DNA damage marker and cleaved-PARP (cl-PARP) as an apoptosis marker; α-tubulin served as the loading control.

(K) Parental and MAPKi-resistant Mel888 cells were treated with 20μM paraquat and/or 2.5 mM NAC for 72 hr. ROS levels were measured using CellROX-Green flow cytometry assay. Relative ROS inductions are plotted.

Error bars in this figure represent as mean ± standard deviations from biological triplicates (*$p \leq 0.05$, **$p \leq 0.01$, ***$p \leq 0.001$, Student's t test).

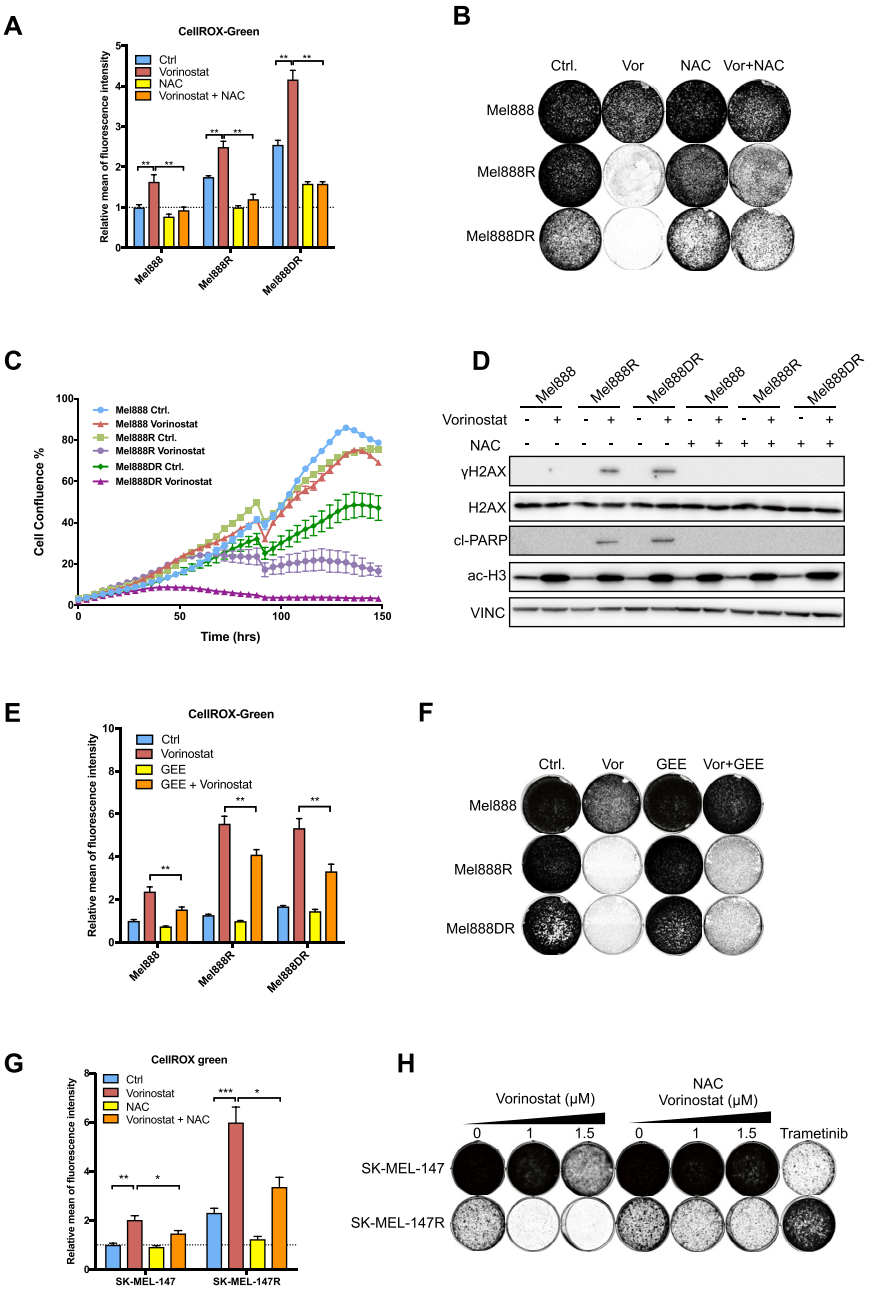

Figure S2. HDACi Is Detrimental to MAPKi-Resistant *BRAF* and *NRAS* Mutant Melanoma Cells, Related to Figure 2

(A) Parental and MAPKi-resistant Mel888 cells were treated with 2 μM vorinostat and/or 2.5 mM NAC for 72 hr. ROS levels were measured using CellROX-Green flow cytometry assay. Relative ROS inductions are plotted.

(B) Long-term colony formation assays of parental and MAPKi-resistant Mel888 cells treated with vorinostat and/or NAC. Cells were seeded 50,000 cells per well in 6-well plates and treated with 1 μM vorinostat and/or 2.5 mM NAC for 8 days. Afterward, the cells were fixed, stained, and photographed.

(C) Incucyte proliferation assay of parental and MAPKi-resistant Mel888 cells, seeded 2,000 cells per well in a 96-well plate and cultured in the presence or absence of 1 μM vorinostat.

(D) Protein lysates were harvest from the MAPKi-resistant and parental Mel888 cells treated with 1 μM vorinostat and/or 2.5 mM NAC for 72 hr. Western blot analysis shows γH2AX as a DNA damage marker and cleaved-PARP (cl-PARP) as an apoptosis marker; α-tubulin served as the loading control.

(E) Parental and MAPKi-resistant Mel888 cells were treated with 2 μM vorinostat and/or 2.5 mM reduced glutathione ethyl ester (GEE) for 72 hr. ROS levels were measured using CellROX-Green flow cytometry assay. Relative ROS levels are indicated.

(F) Long-term colony formation assays of parental and MAPKi-resistant Mel888 cells treated with vorinostat and/or GEE. Cells were seeded 50,000 cells per well in 6-well plates and treated with 1 μM vorinostat and/or 2.5 mM GEE for 8 days. Afterward, the cells were fixed, stained, and photographed.

(legend continued on next page)

(G) *NRAS* mutant melanoma cells SK-MEL-147 and its MEKi-resistant variant SK-MEL-147R cells were treated with 2 μM vorinostat and/or 2.5 mM NAC for 72 hr. ROS levels were measured using CellROX-Green flow cytometry assay. Relative ROS inductions are plotted.

(H) Long-term colony formation assays of parental and MEKi-resistant SK-MEL-147 cells treated with vorinostat and/or NAC. Cells were seeded 50,000 cells per well in 6-well plates and treated with 1 μM or 1.5 μM vorinostat, 2.5 mM NAC and/or 100 nM trametinib for 8 days. Afterward, the cells were fixed, stained, and photographed.

Error bars in this figure represent as mean ± standard deviations from biological triplicates (*$p \leq 0.05$, **$p \leq 0.01$, ***$p \leq 0.001$, Student's t test).

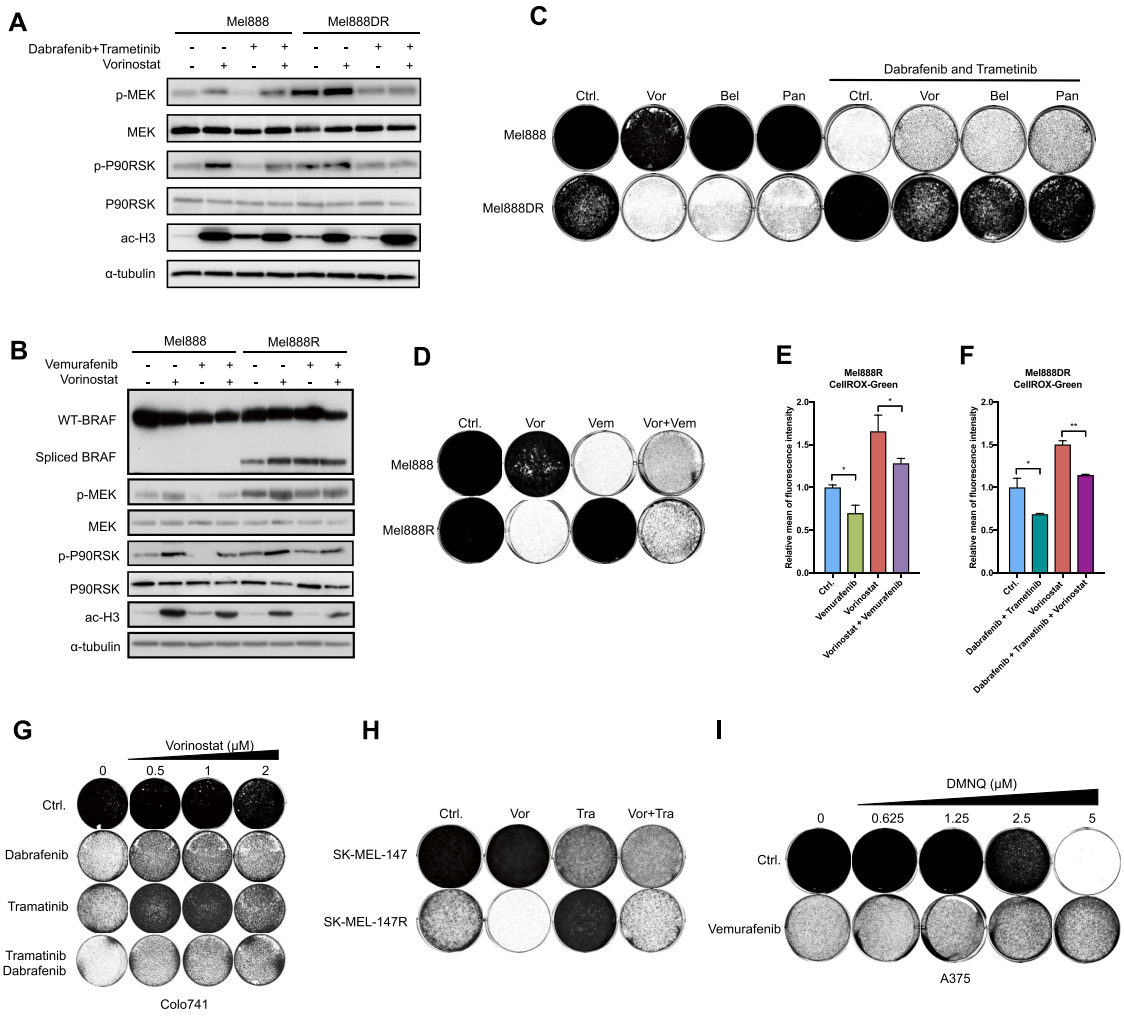

Figure S3. MAPK Inhibition Is Antagonistic with HDAC Inhibition in Additional *BRAF* and *NRAS* Mutant Melanomas, Related to Figure 3

(A) Mel888DR and parental Mel888 cells were treated with 2 μM vorinostat and/or the combination of 0.125 μM dabrafenib and 5 nM trametinib. Protein lysates were harvested after 72 hr. Western blot analysis was performed for p-MEK and p-P90RSK as indicators of activation of MAPK pathway, ac-H3 indicated levels of acetylated histone H3; α-tubulin served as the loading control.

(B) Mel888R and the parental cells were treated with 2 μM vorinostat and/or 0.5 μM vemurafenib for 72 hr. Protein lysates were harvested after 72 hr. Western blot analysis was performed for p-MEK and p-P90RSK as activation of MAPK pathway, ac-H3 indicated levels of acetylated histone H3, Alternative splice variant 61kDa BRAF as the BRAFi-resistance mechanism; α-tubulin served as the loading control.

(C and D) Long-term colony formation assays of parental and MAPKi-resistant Mel888 cells treated with vorinostat and/or MAPKi. (C) Mel888DR and parental cells were seeded 50,000 cells per well in 6-well plates and treated with 1 μM vorinostat (Vor), 0.5 μM belinostat (Bel), 5 nM panobinostat (Pan) and/or combination of 5 nM trametinib and 0.125 μM dabrafenib. (D) Mel888R and parental cells were seeded 50,000 cells per well in 6-well plates and treated with 1 μM vorinostat and/or 1 μM vemurafenib. After 10 days culturing, the cells were fixed, stained, and photographed.

(E and F) Relative ROS level measurements of Mel888R treated with 2 μM vorinostat and/or 2 μM vemurafenib (E), Mel888DR cells with 2 μM vorinostst and/or the combination of 0.125 μM dabrafenib and 5 nM trametinib (F).

(G) Long-term colony formation assays of *BRAF* mutant melanoma cells (Colo741). The cells were seeded 50,000 cells per well in 6-well plates and treated with vorinostat, 5 nM trametinib, 0.125 μM dabrafenib and/or the combinations for 10 days. Afterward the cells were fixed, stained, and photographed.

(H) Long-term colony formation assays of parental and MEKi-resistant SK-MEL-147 cells treated with vorinostat and/or MAPKi. The cells were seeded 50,000 cells per well in 6-well plates and treated with 1 μM vorinostat and/or 50nM trametinib.

(I) Long-term colony formation assays of A375 cells treated with 0.25 μM vemurafenib and indicated concentrations of 2,3-dimethoxy-1,4-napthoquinone (DMNQ) for 10 days.

Error bars in this figure represent as mean ± standard deviations from biological triplicates (*p ≤ 0.05, **p ≤ 0.01, ***p ≤ 0.001, Student's t test).

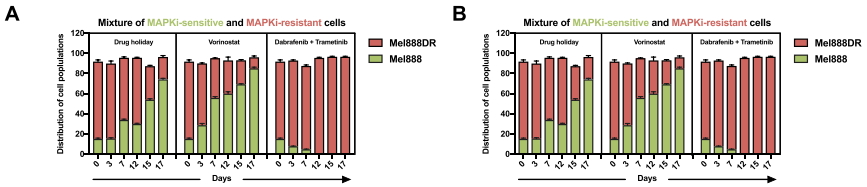

Figure S4. HDACi Is Detrimental to MAPKi-Resistant Mel888 Melanoma, Related to Figure 4

(A and B) MAPKi-resistant cells (RFP+) and their MAPKi-sensitive parental cells (GFP+) were mixed in a 9 to 1 ratio. 2,000,000 cells were seeded in a 10-cm dish and subjected to different treatments. At each time point, the distribution of the cell population was determined using flow cytometry. The ratio of two cell populations at the starting of the experiment (day 0) is indicated. The distribution changes of mixed two cell populations are plotted on the Y-axes against the time on the X-axes. Error bars in this figure panel denoted standard deviations of biological triplicates. The mixture of Mel888DR and Mel888 (A). The mixture of Mel888R and Mel888 (B).

Error bars in this figure denoted standard deviations of biological triplicates.

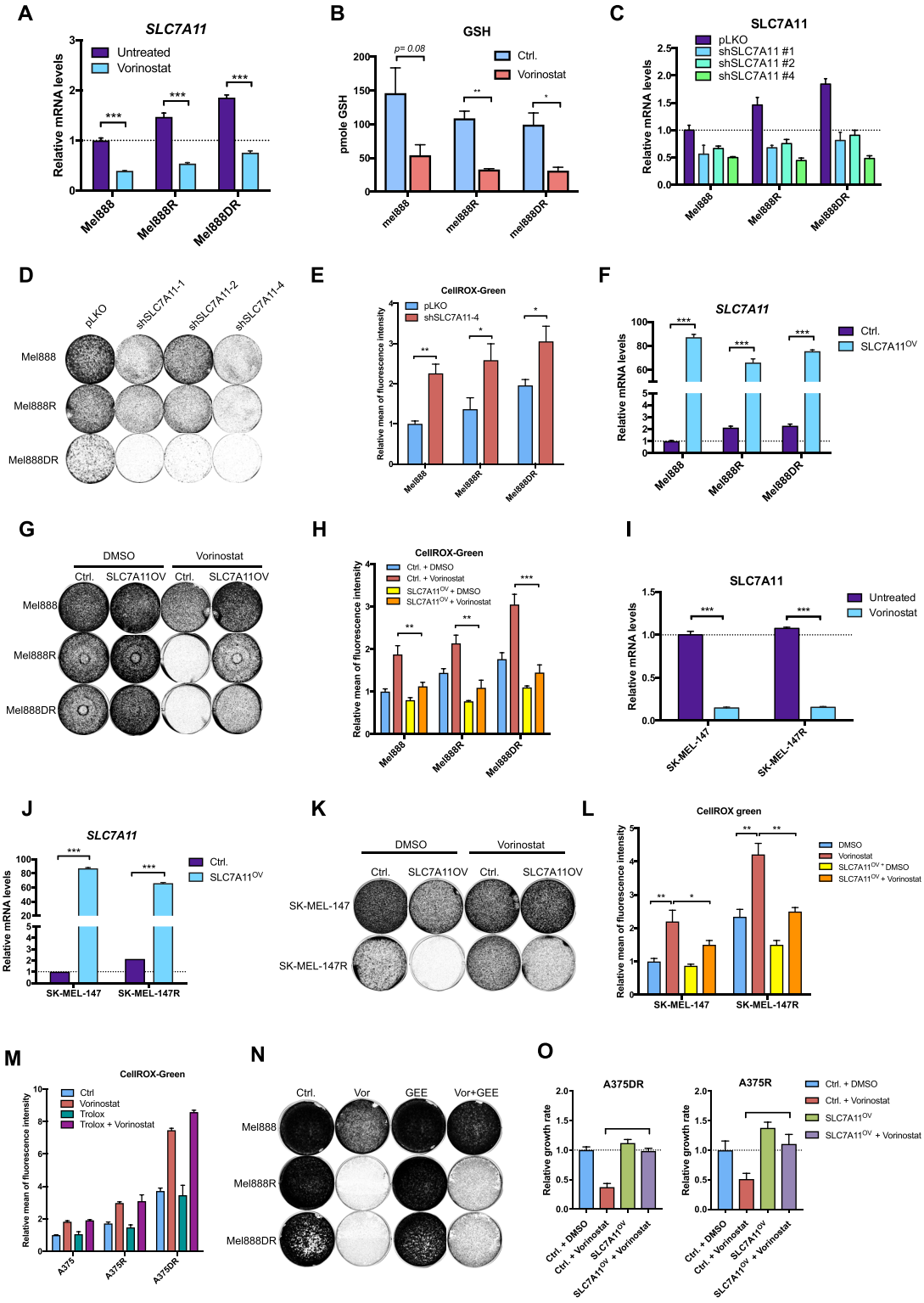

Figure S5. HDACi Suppresses *SLC7A11*, Resulting in ROS Induction in Additional *BRAF* and *NRAS* Mutant Melanoma, Related to Figure 5

(A) mRNA expression analysis of *SLC7A11* measured by qRT-PCR in parental and MAPKi-resistant Mel888 cells treated with 2 μM vorinostat for 48 hr.

(B) Parental and MAPKi-resistant Mel888 cells were treated with 2 μM vorinostat for 72 hr. Total intracellular glutathione (GSH) levels were measured using colorimetric based glutathione detection assay.

(legend continued on next page)

(C–E) Three independent shRNAs targeting *SLC7A11* were individually introduced in parental and MAPKi-resistant Mel888 cells by lentiviral transduction. pLKO empty vector served as the control. (C) The level of *SLC7A11* knockdown by each shRNAs was measured by qRT-PCR. (D) Long-term colony formation of parental and MAPKi-resistant Mel888 cells upon *SLC7A11* knockdown. The cells were seeded 50,000 cells per well in 6-well plate and cultured 10 days. Afterward, the cells were fixed, stained, and photographed. (E) Relative ROS levels in parental and MAPKi-resistant A375 cells upon *SLC7A11* knockdown were measured by CellROX-Green flow cytometry assay.

(F–H) *SLC7A11* was expressed in parental and MAPKi-resistant Mel888 cells by lentiviral transduction. pLX304 empty vector was used as the control (Ctrl.). (F) The levels of *SLC7A11* overexpression in parental and MAPKi-resistant Mel888 cells was measured by qRT-PCR of *SLC7A11* mRNA levels. (G) Long-term colony formation of *SLC7A11* overexpressing parental and MAPKi-resistant Mel888 cells treated with vorinostat. The cells were seeded 50,000 cells per well in 6-well plate and cultured 10 days with or without 1μM vorinostat. Afterward, the cells were fixed, stained, and photographed. (H) *SLC7A11* overexpressing parental and MAPKi-resistant Mel888 cells were treated with 2 μM vorinostat for 72 hr. Afterward, ROS levels were measured using CellROX-Green flow cytometry assay. Relative ROS inductions was plotted.

(I) mRNA expression analysis of *SLC7A11* by qRT-PCR in parental and MEKi-resistant SK-MEL-147 cells treated with 2 μM vorinostat for 48 hr.

(J–L) *SLC7A11* cDNA was expressed in parental and MEKi-resistant SK-MEL-147 cells by lentiviral transduction. pLX304 empty vector was used as the control (Ctrl.). (J) The levels of *SLC7A11* overexpression in parental and MEKi-resistant SK-MEL-147 cells were measured by examining the *SLC7A11* mRNA levels by qRT-PCR. (K) Long-term colony formation of *SLC7A11* overexpressed parental and MEKi-resistant SK-MEL-147 cells treated with vorinostat. The cells were seeded 50,000 cells per well in 6-well plate and cultured 10 days with or without 1μM vorinostat. Afterward, the cells were fixed, stained, and photographed. (L) *SLC7A11* overexpressing parental and MEKi-resistant SK-MEL-147 cells were treated with 2 μM vorinostat for 72 hr. Afterward, ROS levels were measured using CellROX-Green flow cytometry assay. Relative ROS inductions are plotted.

(M) Parental and MAPKi-resistant A375 cells were treated with 2 μM vorinostat and/or 0.25 mM 6-hydroxy-2,5,7,8-tetramethylchroman-2-Carboxylic Acid (Trolox) for 72 hr. ROS levels were measured using CellROX-Green flow cytometry assay. Relative ROS levels are indicated.

(N) Long-term colony formation assays of parental and MAPKi-resistant A375 cells treated with vorinostat and/or Trolox. Cells were seeded 50,000 cells per well in 6-well plates and treated with 1 μM vorinostat and/or 0.25 mM Trolox for 8 days.

(O) The relative growth rate of the responsiveness to 1 μM vorinostat treatment in MAPKi-resistant A375 cells with and without SLC7A11 overexpression. The growth rates were calculated based on the slope a curve fitted through the linear range of the log-transformed confluence measurements from Incucyte date of Figures 5J and 5K. For each cell line, the growth rates were normalized to the mean of the untreated controls. The growth rate of untreated control was considered as a basal line and normalized to 1. The relative growth rates of all growth rates of the drug-treated and genetic manipulated arms were compared with the untreated control arm.

Error bars in this figure represent as mean ± standard deviations from biological triplicates (*$p \leq 0.05$, **$p \leq 0.01$, ***$p \leq 0.001$, Student's t test).

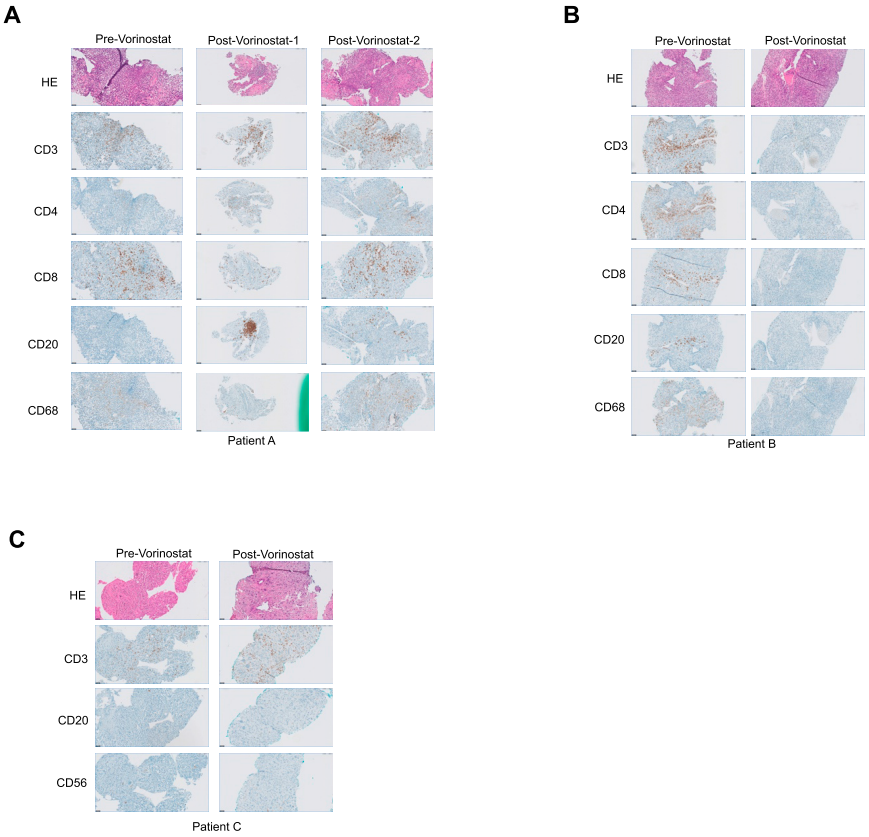

Figure S6. Immune Cells Staining on the Biopsies from Vorinostat-Treated MAPKi-Resistant Melanoma Patients, Related to Figure 7

(A–C) Immunohistochemical staining of immune cells in melanoma tissue section from MAPKi-resistant melanoma patients (A–C) pre- and post-treated with vorinostat as indicated. CD3 served as a pan-T cell marker. CD4 served as a T helper cell marker. CD8 served as killer T cells. CD20 served as a B cell marker. CD68 served as a macrophage marker. The black bar in the lower left corner represents 50 μm.